Applied Magnetic Resonance (2024) 55:1481–1514
https://doi.org/10.1007/s00723-024-01713-4

Applied
Magnetic Resonance

REVIEW

Nitroxide Spin Labels for Exploring Relationships Between Molecular Structure, Microenvironment and EPR Parameters: A Mini-review Dedicated to Carlo Corvaja

Klaus Möbius[1] · Anton Savitsky[2] · Martin Plato[1] · Wolfgang Lubitz[3]

Received: 14 August 2024 / Revised: 30 August 2024 / Accepted: 31 August 2024 /
Published online: 14 September 2024

Abstract

This mini-review is dedicated to Carlo Corvaja (University of Padova) in recognition of his important contributions to the study of biomimetic donor–acceptor model dyads and triads and to the understanding of spin exchange in excited fullerene–nitroxide derivatives. We report on attractive examples of multi-frequency and multi-resonance EPR spectroscopy, highlighting recent work in Padova and Berlin/Mülheim. The examples selected include TR-EPR, ENDOR, and EDNMR experiments on photoexcited spin-labeled macromolecules, such as fullerene–nitroxide complexes or photosynthetic bacterial reaction centers, which were optionally NO spin-labeled. From the spin interaction parameters measured, detailed information about structure and dynamics of macromolecules embedded in liquid-solution or solid-state microenvironments could be extracted.

Prologue

We dedicate this mini-review to Prof. Carlo Corvaja (University of Padova) on the occasion of his 85th birthday (which actually had been celebrated already in 2022).

✉ Klaus Möbius
moebius@physik.fu-berlin.de

✉ Anton Savitsky
anton.savitsky@tu-dortmund.de

✉ Wolfgang Lubitz
wolfgang.lubitz@cec.mpg.de

[1] Department of Physics, Free University Berlin, Arnimallee 14, 14195 Berlin, Germany

[2] Faculty of Physics, Technical University Dortmund, Otto-Hahn-Str. 4a, 44227 Dortmund, Germany

[3] Max-Planck-Institute for Chemical Energy Conversion, Stiftstr. 34-36, 45470 Mülheim an der Ruhr, Germany

Carlo Corvaja (born July 25, 1937)
[Photo: Fabio Corvaja, 2024].

Q: When did you meet Carlo Corvaja for the first time and where was it?
A: It was almost 60 years ago, when the German Mark (DM) was equivalent to 156 Italian Lira (ITL) and Martin Plato, Klaus Möbius and Carlo Corvaja were 29 ± 1 years old. In addition, it was in England.

The first encounter of Klaus Möbius and Martin Plato with Carlo Corvaja was in March 1965 when they attended the international EUCHEM Conference on "Chemical Aspects of Electron Spin Resonance" in Cirencester (England). It was the first international conference in our young EPR career. We enjoyed the opportunity to talk with high-profile EPR researchers, among them Jack Freed, Jim Hyde, Fabian Gerson, Joan van der Waals, Vladislav Voevodsky, Giovanni Giacometti—and his graduate student Carlo Corvaja.

Together with Pier Luigi Nordio and Marina Brustolon, Carlo Corvaja was among the first-generation members of the renowned Padova group of Giovanni Giacometti, who had pioneered EPR spectroscopy in Italy. It was no surprise then that the group members knew (almost) everything about EPR spectroscopy. But beyond that, they had an amazing knowledge of political, scientific and medical history. They were fond of old maps and historic books, and were fascinated by antique scientific instruments. They were familiar with the behavior of snakes and birds and watched them in the free nature. They were involved in the preservation of Cultural Heritage using up-to-date physico-chemical tools. In addition, they admired the masterful craftsmanship of finely chiseled contemporary gold jewelry made from thin gold filaments. What a stimulating environment for guest scientists! In addition, all this against the background of the day-to-day excitement

Galileo Galilei (From: THE EDWARD WORTH LIBRARY, Dublin)

Fig. 1 Galileo Galilei (1564–1642). He was a teacher at the University of Padova from 1592 to 1611. Padova University, founded in the year 1222, is one of the oldest in the world. Galileo Galilei is considered the founder of modern science. He accomplished numerous seminal discoveries in Padova. For example, with his novel telescope, he observed the four largest satellites of Jupiter (1610). His priority of the invention of scientific instruments is not always undisputed [1]. (The etching is from the Edward Worth Library in Dublin, Ireland)

of an extended teaching and research stay at the University of Padova, one of the oldest universities in the world; the place where Galileo Galilei had worked as a teacher and researcher (see Fig. 1). In addition, the place which is also famous for its ancient Medical Faculty (see Fig. 2). Where you can see an important section of the history of medicine, that of anatomy including public dissection of human corpses. For teaching purposes, they were carried out there in early times of the

Fig. 2 The University of Padova is famous also for its ancient Medical Faculty, which attracted scholars from all over Europe in the Middle Ages and the Renaissance. The university's main building, Palazzo del Bo, houses the old anatomical theater built by Girolamo Fabricius D'Acquapendente in 1584. This is probably the first permanent anatomical theater known to history. The elliptical-shaped theater has six tiers carved from walnut and can accommodate up to 300 spectators. The seating is arranged so that each student would have an uncompromised view of the dissecting table. Public dissections of human corpses were often carried out under candlelight. (The picture was taken by an unknown photographer)

Middle Ages and the Renaissance, under suspicious surveillance by the Catholic Church.

1 Introduction

In the subsequent decades after their first encounter in 1965, Carlo Corvaja and K. M., together with their respective co-workers, were orbiting independently around their common center of gravity, which was EPR spectroscopy. They did so in various sub-worlds of EPR spectroscopy, predominantly "Spin Chemistry" and "ENDOR", where they met again and again at intersections of biologically inspired photo-chemistry and photo-physics. Occasionally, they also met at visits of EPR laboratories and conferences all over the world. Unforgettable for us, in Padova, Venice, Berlin, Kazan—and on the island of Rhodes, where Carlo Corvaja received the 2001 Silver Medal Award in Chemistry from the International EPR Society. Whenever they encountered, they enthusiastically discussed their ideas of science and society, democracy and tyranny. No less enthusiastically, their ideas of peace and justice, the arts and history. Then they would return to their various sub-worlds. But always looking forward to their next encounter to exchange new ideas and old experiences.

In Spin Chemistry as well as in ENDOR, the decisive quantum phenomena have their origin in weak magnetic interactions within and between reaction partners. In photoreactions, the reaction partners are often transient and/or stable paramagnetic intermediates of radical and triplet chemistry. The resulting characteristic electron- and nuclear-spin polarization phenomena of the intermediates can be observed in the EPR spectra. By analyzing the spectra, the quantum mechanical control mechanisms of fundamental (bio)chemical reaction pathways can be revealed.

With Carlo Corvaja and his co-workers in Padova, we share common interests in EPR spectroscopy of transient states in (bio)chemistry, e.g., photosynthetic systems and their biomimetic model complexes. However, while our main interest was in photosynthetic *Reaction Centers* for light-induced *charge* separation of chlorophyll–quinone donor–acceptor complexes, Carlo Corvaja was primarily interested in photosynthetic *Antenna* complexes for light-induced *energy* transfer. For instance, the mechanisms of light-induced singlet–singlet and triplet–triplet energy transfer between carotenoids and chlorophyll pigments. An exemplary publication by the Padova group with Donatella Carbonera, Marilena di Valentin, Carlo Corvaja, Giovanni Giacometti, Giancarlo Agostini, and their co-workers from the Arizona State University group with Paul A. Liddell, Ana L. Moore, Thomas A. Moore, and Devens Gust is Ref. [2]. There, carotenoid triplet detection by time-resolved transient EPR (TR-EPR) spectroscopy in carotenopyropheophorbide dyads (see Fig. 3) is described. The TR-EPR technique, when combined with laser photolysis, provides detailed information on reactive species in their excited states.

Carotenoid triplets play a photoprotective role in natural photosynthesis. The main process of carotenoid triplet formation is known to be triplet–triplet energy transfer from chlorophyll triplets. The structural requirements for high transfer yields are still an active field of research and the presence of competitive triplet formation pathways has not been excluded. Transient EPR measurements of triplet states formed by photoexcitation allow detection of the initial spin polarization. The characteristic polarization pattern derives from the mechanism of triplet formation. In the case of triplet–triplet energy transfer, if the condition of spin angular momentum conservation is fulfilled, simulation of the EPR spectra gives information about the donor–acceptor mutual orientation. In their publication, Corvaja et al. describe transient EPR experiments on two artificial photosynthetic dyads, consisting of a carotenoid covalently linked to a free-base or zinc-substituted pyropheophorbide moiety. The results are discussed in terms of possible dyad conformations owing to the flexibility of the linker bridge.

Carotenoids act as light-harvesting pigments and photoprotectants in photosynthetic organisms. Their role as *antenna pigments* is accomplished by absorption of photons in the blue-green spectral range, followed by rapid singlet–singlet energy transfer to chlorophyll pigments. The *photoprotective function* involves the direct quenching of singlet oxygen or the quenching of chlorophyll triplets that could sensitize the formation of singlet oxygen. The process of chlorophyll triplet quenching is generally regarded as triplet–triplet energy transfer from chlorophyll to carotenoids.

Energy transfer has been widely studied in photosynthetic organisms, including both bacteria and higher plant systems. In parallel, investigations of artificial

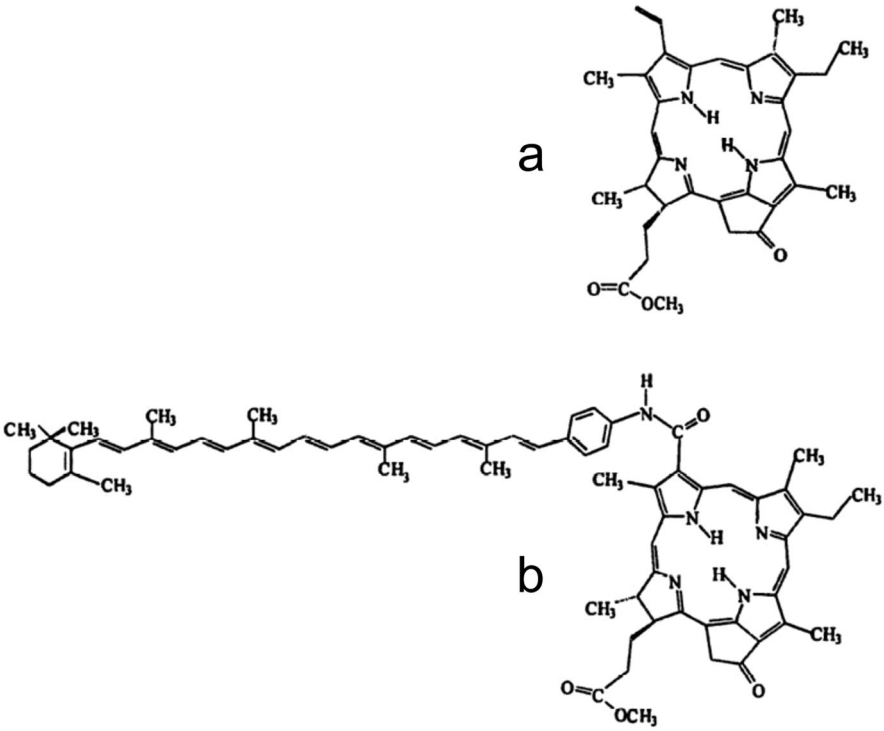

Fig. 3 Molecular structure of **a** free-base pyropheophorbide and **b** free-base carotenopyropheophorbide. The zinc pyropheophorbide and the zinc caroteno-pyropheophoride have the same molecular structures as the corresponding free-base compounds except for the substitution of the central protons with zinc [2]

photosynthetic systems have been carried out on molecular dyads and triads consisting of carotenoid polyenes covalently linked to porphyrin and chlorophyll derivatives. These artificial systems can mimic both the antenna and photoprotective functions.

It has been shown that the spin angular momentum is conserved during the transfer process. The relative populations of the triplet acceptor sublevels are proportional to the squares of the projections of the donor principal magnetic axes on the acceptor magnetic axes. It is therefore possible for the chemical synthesis of the dyads to determine the conformational requirements of the model compounds for an efficient triplet–triplet energy transfer.

The transient triplet-state EPR spectra of the free-base pyropheophorbide and of the zinc pyropheophorbide are shown in Fig. 4a and b, respectively. The spectra have been detected at 0.6 μs delay after the laser flash. They are spin-polarized in an EAEAEA and AAEAEE fashion, respectively.

The analysis of the experimental results has been performed in terms of spin angular momentum conservation during triplet–triplet energy transfer from the pheophorbide triplet to the carotenoid triplet in an external magnetic field.

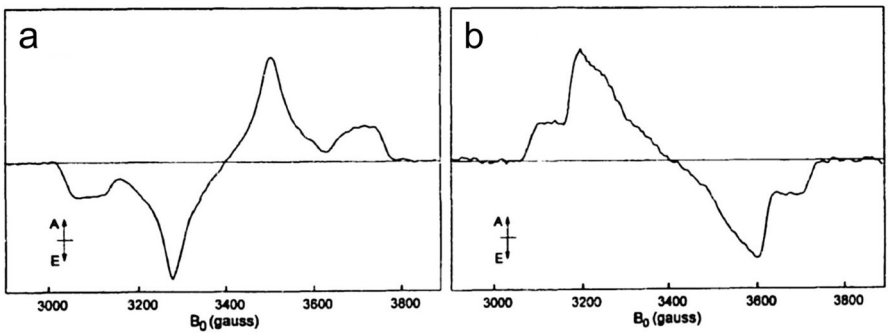

Fig. 4 Time-resolved triplet-state EPR spectra recorded by direct detection of **a** free-base pyropheophorbide, **b** zinc pyropheophorbide in 2-methyltetrahydrofuran. $T = 20$ K, $P_{MW} = 14.5$ mW, delay time after the laser pulse = 0.6 μs, integration gate = 0.3 μs. A and E stand for absorption and emission, respectively. Figure taken from Ref. [2]

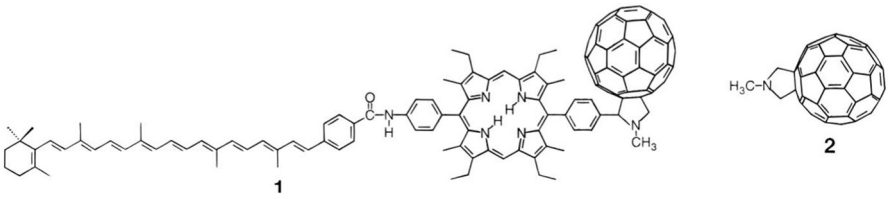

Scheme 1 Carotene-porphyrin-fullerene triad 1 and functionalized fullerene moiety 2, see ref. [3]

The authors conclude that the widely different initial polarization of the carotenoid triplet formed in a light-excited carotenopyropheophorbide, observed in the presence and absence of a Zn atom in the center of the porphyrin ring, are certainly not only due to the well-known differences in the population kinetics of the porphyrin moiety following metalation. Different conformations have to be invoked in order to account for the experimental data. Apparently, the test of the conformational change explanation requires additional experiments regarding the possibility of different mechanism to be invoked in the birth of the triplet. For a detailed discussion of this issue, see Ref. [2].

An important step forward towards rigid donor–acceptor model systems was achieved by the same Padova/Arizona groups with the synthesis of a carotene–porphyrin–fullerene triad (see Scheme 1), and the analysis of the TR-EPR spectra of its transient radical-pair intermediate after laser-flash excitation [3].

This publication is an exciting piece of science about the essence of the photochemical experiments on molecular donor–acceptor triads consisting of a porphyrin (P) covalently linked to a carotenoid polyene (C) and a fullerene derivative (C_{60}). The triads have been studied at 20 K by time-resolved EPR spectroscopy following light excitation by short laser-flashes. Excitation of the porphyrin moiety yields C—^{1}P—C_{60}, which decays by photoinduced electron transfer to yield C—P$^{\bullet+}$—$C_{60}^{\bullet-}$. This state rapidly evolves into a final charge-separated radical pair (RP) state $C^{\bullet+}$—P—$C_{60}^{\bullet-}$ whose spin-polarized EPR signal was detected and simulated.

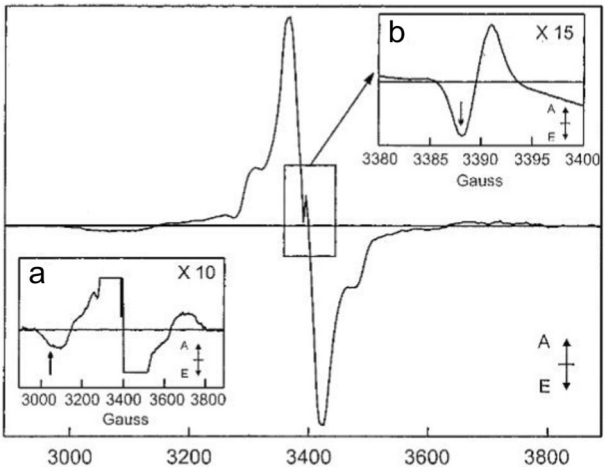

Fig. 5 Time-resolved EPR spectrum of triad **1** in 2-methyltetrahydrofuran. The spectrum was obtained at 20 K, 0.4 μs, integration gate = 0.3 μs after the laser excitation pulse with 14.5 mW of microwave power and an integration time of 0.2 μs per point. The direct-detection spectrum appears in absorption (*A*) or emission (*E*), as indicated. **a** Expansion of the spectrum in the carotenoid triplet region. **b** Expansion of the spectrum of the $C^{\cdot+}$—P—$C_{60}^{\cdot-}$ radical pair (1 G = 10^{-4} T) (figure taken from Ref. [3])

The exchange interaction between the electrons in the radical pair is rather weak ($J = 1.2$ G). The RP $C^{\cdot+}$—P—$C_{60}^{\cdot-}$ decays to give the carotenoid triplet in high yield with a time constant of 1.2 μs. The spin polarization of ^{3}C—P—C_{60} is characteristic of a triplet formed by charge recombination of a singlet-derived radical pair. The kinetics of the decay of ^{3}C—P—C_{60} to the ground state were also determined. The photoinduced electron transfer from an excited singlet state at low temperature and the high yield of charge recombination to a spin-polarized triplet indeed mimic similar processes observed in photosynthetic reaction centers.

Most of the photosynthetic reaction center models have employed quinones, porphyrins, or aromatic imides as electron acceptor moieties. However, it has been found recently that also fullerenes can function in this way. For example, a variety of molecular dyads consisting of fullerenes linked to donor pigments demonstrate photoinduced electron transfer to the fullerene, yielding a charge-separated RP state, see Ref. [2].

In Fig. 5, it is shown that Triad **1** (see Scheme 1) has undergone photoinduced electron transfer at low temperatures, followed by charge recombination to a triplet state, similar to natural photosynthetic reaction centers. In the present study, TR-EPR was used to observe transient triplet and radical-pair states, their spin polarization, and their kinetic properties in order to compare the behavior of **1** with that of reaction centers and other model compounds.

In their Conclusions the authors emphasize that their TR-EPR studies on Triad **1** are in complete accord with the results of their earlier optical studies. Excitation of the porphyrin moiety is followed by photoinduced electron transfer from the first excited singlet state to yield an intermediate charge-separated state, which evolves into a final radical pair state that can be detected by TR-EPR. The RP state mainly

decays to the carotenoid triplet, $^3C{-}P{-}C_{60}$, which then decays to the ground state. These events occur not only in solution at ambient temperatures, but also in a glass matrix at temperatures as low as 10 K. The temperature dependence of the charge-recombination reaction is extremely weak.

The EAA EEA spin polarization pattern of the carotenoid triplet EPR signal is characteristic of a triplet formed by recombination of a singlet-born radical pair, rather than by normal spin–orbit coupling induced intersystem crossing.

It should be noted that all previous reaction center models employing pigments related to natural chlorophylls and carotenoids have demonstrated charge recombination to the ground state, rather than radical-pair induced triplet formation. In addition, the vast majority of these model systems failed to undergo photoinduced electron transfer in glasses at low temperatures.

Comparison of the results for **1** with those for other triads suggests that the unusual properties of **1** must derive from the fullerene moiety and associated reorganization and stabilization energies, rather than from differences in oxidation and reduction potentials and energies of excited states as measured in polar solvents. For a detailed discussion of this important work, see Ref. [3].

Somehow, it is surprising that we do not have joint publications with Carlo Corvaja in which model systems mimicking primary photosynthesis are discussed. Donor–acceptor dyads and triads as model systems for light-induced electron-transfer processes have long been the subject of our research. This research was carried out in close collaboration with the group of Harry Kurreck at the Chemistry Department of FU Berlin [4–6].

In recent years, Carlo Corvaja's favorite research area in Padova had shifted to *Fullerene derivatives*, specifically, to electron spin polarization effects in triplet, quartet and quintet states of fullerenes linked to one or more free nitroxide radicals [7]. In Berlin/Mülheim, our favorite research areas were photosynthetic *Reaction Centers* (RCs) and their interactions with the microenvironment. In this mini-review, we will focus on nitroxide spin-labeled protein complexes for which the research areas of Padova and Berlin/Mülheim overlap to a certain extent. We have singled out a few examples from both groups that we find particularly interesting. The common link between the selected examples is time-resolved single- or multiple-resonance EPR spectroscopy of light-irradiated macromolecules with short-lived doublet- or excited-state intermediates. The experiments are designed for investigating the relationships between molecular structure, microenvironment of the paramagnetic cofactors and their EPR properties [8, 9].

In Padova, the X-band TR-EPR measurements employed a Nd:YAG pulsed laser (second harmonic, $\lambda = 532$ nm) to illuminate the sample for times as short as 5 ns. Using fullerene molecules linked to one or more nitroxide radicals, the Corvaja group was able to observe photoexcited species with one, two, three, and four unpaired electron spins. The aim of their studies was to understand the basic processes for photogeneration of high-spin organic molecules. The ultimate goal was to develop viable methods for controlling and modulating molecular magnetism by means of light beams.

In Berlin/Mülheim, we have capitalized on the improved spectral resolution of high-field EPR spectroscopy, primarily at W-band (TR-EPR, ENDOR, and

EDNMR). The experiments were carried out in combination with selective isotope labeling to explore fundamental light-driven primary processes in bacterial reaction centers (bRCs). In certain cases, to elucidate subtle protein–water interactions with the solvent matrix, site-directed nitroxide spin labeling (SDSL) of the bRCs was used. Thereby, the relationships between the microenvironment of the spin label at the protein surface and molecular magnetic parameters were explored in detail. Ultimately, our aim was to gain new insights into the interconnections between structure and function of electron-transfer cofactors embedded in their protein matrix.

2 Examples

2.1 *Examples from Padova*: Time-Resolved EPR of Single and Double Spin-Labeled C_{60} Fullerene Derivatives. Observation of Triplet, Quartet and Quintet Excited States in Liquid and Solid Solutions

In the Chemistry Department of Padova University, the Corvaja group has extensively studied, by TR-EPR, the magnetic properties of C_{60} fullerenes (Fig. 6) linked to stable nitroxide radicals. Molecular magnetism in organic complexes obviously occurs when there is an odd number of electrons in the complex, as is the case of free radicals. Alternatively, it occurs in certain molecular high-energy states

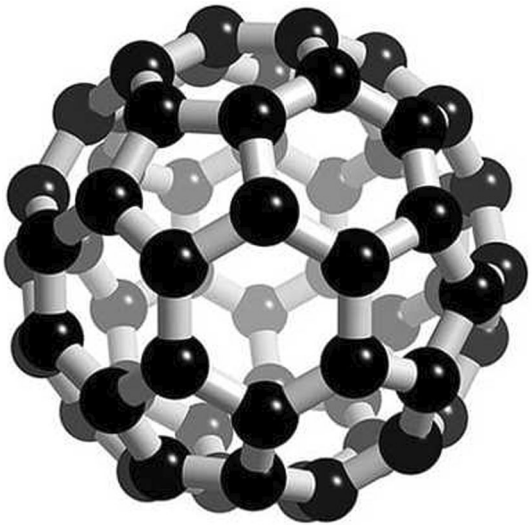

Fig. 6 Structure of the all-carbon molecule C_{60} fullerene (ball-and-stick model). It is comprised of 12 regular pentagonal faces and 20 regular hexagonal faces. The 60 carbon atoms are placed at the vertexes. The carbons of fullerenes are bound together to form closed cage structures. The fullerenes were discovered in the early 1990s years (Nobel Prize in Chemistry 1996 to Robert F. Curl, Jr., Harold W. Kroto, and Richard E. Smalley). Fullerenes are formed in a variety of ways when carbon is heated to high temperatures in an inert atmosphere. The product obtained contains several different fullerenes, but the one with the highest yield consists of 60 C atoms bound together in a truncated icosahedron structure

that are populated by the absorption of light. It is required that the electron spins in the excited molecule and in the radical partner couple in a way that a magnetic moment is created (total spin $S>0$). When photoexcited in the nanosecond range, fullerene–nitroxide derivatives combine both sources of molecular magnetism. The mechanism of this spin–spin coupling was explored by analyzing the line shapes and decay times of the TR-EPR spectra of the different fullerene derivatives.

The TR-EPR research on fullerene derivatives in Padua was partly carried out in close collaboration with Seigo Yamauchi and his group who worked on related subjects at the Tohoku University in Sendai. Important references of this work are, for instance, [10–14].

Fullerene C_{60} molecules have a series of interesting properties connected with their capability to accept one extra electron from nearby donors and to form paramagnetic excited states by light absorption [15]. For example, when a mixture of fullerene and a donor polymer is illuminated by visible light, an electron is transferred from the donor to C_{60} and two charged radicals are formed. Such a charge separation process is exploited in organic photovoltaic devices [16].

Since long, nitroxide radicals, for example TEMPO [17], have been inserted as spin labels in a variety of molecular systems to study structural and dynamic properties [8, 9]. The unpaired electron predominantly resides on the NO group, i.e., delocalization on other atoms including the nearest neighbors is practically zero. However, population of the high-energy levels as well as the decay pathways and rates of the excited states can be strongly affected by the presence of the nitroxide unpaired spin. This is due to interactions with other electron spins. Although the coupling is small, it can give rise to large effects on the line intensity distribution in the magnetic resonance spectra [10, 11, 13, 18, 19]. To illustrate this, C_{60} chromophores labeled with one or two nitroxide spins were examined in their light-excited state [13, 20].

As a chromophore, C_{60} has various favorable characteristics which are preserved in C_{60}-nitroxide derivatives: (i) a long-lived excited triplet state produced with high yield, (ii) chemical stability in the excited state, (iii) absence of magnetic nuclei (neglecting ^{13}C in the low natural abundance of about 1%). These properties facilitate the observation of the excited state and simplify the EPR spectrum. This makes the analysis of the spectrum unambiguous because only the hyperfine structure due to the nitrogen nuclei of the spin label occurs.

The Corvaja group made the first observation of radical–triplet pairs in the quartet and quintet states of spin-labeled C_{60} derivatives both in liquid solution and frozen matrix [14]. The g factor and the hyperfine structure of the radical pairs are indicative of the spin multiplicity and were used to assign the total spin state of the excited complex.

The Corvaja paper reviewed here presents the results of a thorough TR-EPR investigation of four C_{60} derivatives Ia and Ib, IIa and IIb, spin-labeled with one or two TEMPO radicals, respectively. Their chemical structures are shown in Fig. 7. The fulleropyrrolidines [21] were studied in their (dark) ground state by cw EPR, and by TR-EPR in their photoexcited states after ns-pulsed laser excitation, see Figs. 8 and 9.

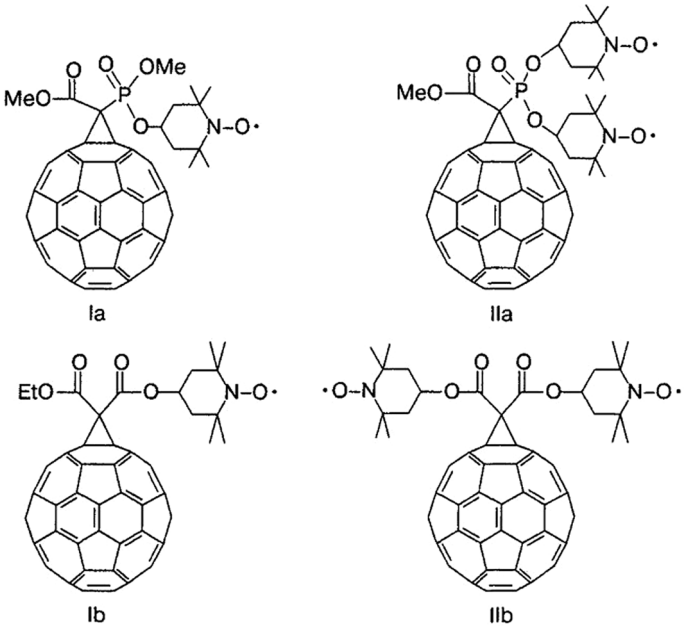

Fig. 7 Spin labeled fullerene derivatives (fulleropyrrolidines) studied by the Corvaja group [14, 22]. Shown are monoradical (Ia, Ib) and biradical (IIa, IIb) fullerene derivatives, linked together at different distance and relative orientation to each other

In the primary stages of numerous chemical and photochemical reactions, radical pairs (RPs) and radical–triplet pairs (RTPs) are formed which eventually evolve to reaction products. Time-resolved EPR spectroscopy of these species is feasible, even if they are present in solution at low stationary concentration. This is due to the spin polarization of the radical species in the early instants of their formation, which strongly enhances the EPR sensitivity.

The strongly spin-polarized TR-EPR signals are the superposition of the spectra of ^{4}[RTP] and of RP. The spectrum of RP is characterized by three lines separated by about 15 G and centered at $g = 2.006$. The spectrum of ^{4}[RTP] consists of three lines centered around $g = 2.003$ with a hyperfine splitting of about 5 G. The signals occur either in Emission or in enhanced absorption and eventually change polarization as they evolve on timescales of a few microseconds.

Let us summarize the results of the 2006 papers [14, 22] from the Corvaja group on time-resolved EPR spectra of two single spin-labeled and two double spin-labeled C_{60} derivatives dissolved in liquid and frozen solutions. The spectra were observed after pulsed laser excitation with ns time resolution. Quartet and quintet excited species were identified which arise from the electron spin–spin exchange coupling J of the triplet-excited fullerene moiety with the unpaired spin(s) of the nitroxide label(s). Despite rather similar molecular structures in both series of single and double labeled derivatives (see Fig. 7), a very different behavior of the TR-EPR

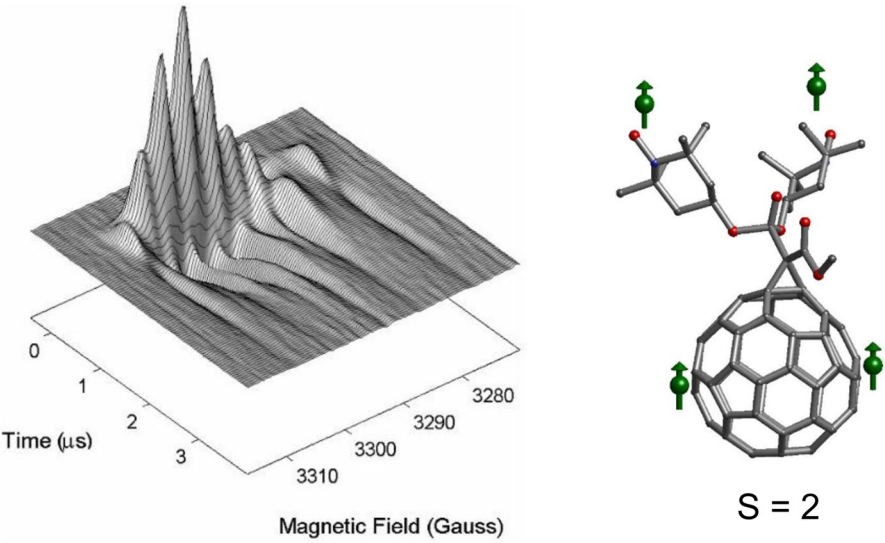

Fig. 8 X-band TR-EPR (3D presentation) of a C_{60} derivative bearing two stable nitroxide radicals (structure IIa in Fig. 7) after light excitation at 290 K in liquid toluene solution. The spectrum is recorded by direct detection (i.e., without field modulation and lock-in detection, but with broad-band preamplification and data collection by a fast digital oscilloscope). The transient EPR spectrum is extracted 0.5 μs after the laser pulse (fired at time = 0). The spectrum appears in enhanced absorption (above the noise floor) immediately after the laser pulse, later in emission (below the noise floor). It is assigned to a quintet electron spin state ($S = 2$, four unpaired electrons). Adapted from Refs. [14, 22]

spectra was found. This is due to a substantial difference of the exchange coupling energy in the monoradicals Ia and Ib compared to the biradicals IIa and IIb.

In liquid solution at room temperature, the EPR spectra of derivatives Ia and Ib in their electronic ground state consist of three lines due to the ^{14}N hyperfine coupling. They are further split by the small hyperfine coupling of the nitroxide methyl protons. When these derivatives are photoexcited, strong TR-EPR signals of different lineshape are recorded. They were analyzed on the basis of the formation of quartet states generated by the coupling of the $S = 1$ spin on the fullerene moiety with the radical nitroxide $S = 1/2$ spin (systems Ia and Ib).

The room temperature EPR spectra of IIa and IIb in the electronic ground state present three additional lines between the three hyperfine components typical of the nitroxide monoradicals. The spectral simulation is consistent with the presence of two weakly exchange-coupled nitroxide groups. After pulsed laser photoexcitation, the TR-EPR spectra show an absorption/emission (A/E) pattern which were analyzed in terms of spin-polarized quintet states ($S = 2$) [22]. The electron exchange interaction J in radical pairs is an important parameter. Its value and sign determine the polarization pattern, the kinetic behavior, and the magnetic field effects on reactivity [23–28].

When a laser light pulse with wavelength $\lambda \approx 500$ nm is absorbed by the C_{60}, the fullerene is promoted to the first excited singlet state S_1. Because of the attached nitroxide groups, the spin multiplicity of the whole molecule in this state

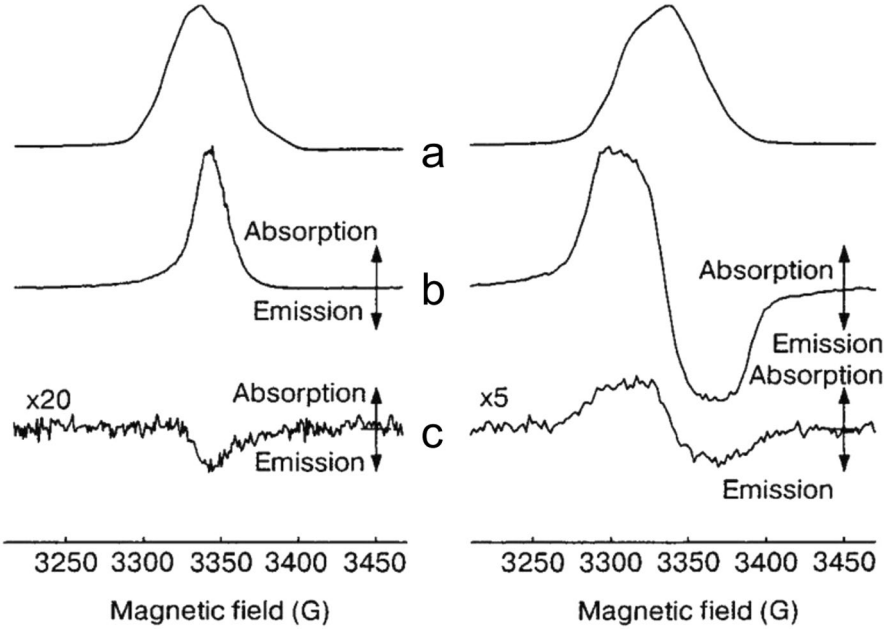

Fig. 9 X-band EPR spectra of biradicals IIa (left panel) and IIb (right panel) recorded in glassy matrix of toluene at 120 K. **a** Integrated EPR spectra recorded in the dark. **b** TR-EPR spectra recorded at 0.4 μs after the laser pulse, **c** TR-EPR spectra recorded at 70 μs after the laser pulse (from Ref. [22])

is a doublet for the monoradicals Ia and Ib, and a mixed singlet–triplet state for the biradicals IIa and IIb. Intersystem crossing (ISC) is caused by spin–orbit and spin–spin exchange interactions of the unpaired electrons of the nitroxide with those in the fullerene SOMOs. This generates a number of electronic states characterized by triplet excitation on the C_{60} part, which interacts only weakly with the nitroxide spin states. In a profound quantum mechanical analysis, the Corvaja group has shown that the TR-EPR spectra of nitroxide spin-labeled fullerenes can be understood on the basis of the total spin Hamiltonian [22]:

$$\mathcal{H} = \mathcal{H}_Z + \mathcal{H}_{hyp} + \mathcal{H}_{exch} + \mathcal{H}_{dip}$$

where the first term on the right is the Zeeman interaction of the triplet state and of the radical(s); the second term is the hyperfine interaction term, which involves only the spin of the nitroxide groups of the radicals, neglecting the small coupling with ^{13}C nuclei of the fullerene cage. The third term of the Hamiltonian comprises the exchange interaction between the triplet and the radical, and in the case of IIa and IIb, it also includes the exchange term between the radicals. The last term of the Hamiltonian represents the dipolar interaction between the triplet electron spin and the nitroxide spins. The magnitude of the electron exchange interaction between the two unpaired electrons in the ground state is obtained from the analysis of the EPR spectra in the dark.

In case of the quintet excited state, the assignment was confirmed by measuring the frequency of the echo-detected transient nutation. Fourier transformation of the transient spectra along the microwave pulse length allowed to disentangle the quintet transitions and to obtain precise measurements of the zero-field splitting parameters.

Single and double nitroxide spin-labeled C_{60} derivatives in frozen matrices give quite different TR-EPR spectra depending on the magnitude of the exchange interaction between the unpaired spins on the triplet fullerene moiety and the nitroxide radical spin(s). In the fullerene derivatives Ib and IIb, where the nitroxide radical is bound to a malonate ester, the exchange coupling is weak and the frozen-solution TR-EPR spectra are very similar to those of triplet-excited fullerene monoadducts. In the phosphorylated methanofullerenes Ia and IIa, a strong spin–spin coupling is found probably caused by super-exchange promoted by the phosphorus atom. The frozen-solution spectra show the typical features of a quartet state (for the single labeled derivative) and of a quintet state (for the double labeled derivative).

As far as we know, this is the first determination of the magnitude and sign of the radical-triplet exchange coupling J in a radical-triplet pair (RTP).

For Ia, J_{RTP} is negative and its absolute value is large compared with the nitroxide ^{14}N hyperfine coupling. For both IIa and IIb in solution, the Corvaja group observed a quintet state arising from the exchange coupling of the fullerene triplet spins with the spins of the two nitroxides. From computer simulation of the TR-EPR spectra, a negative value of the radical–radical exchange interaction J_{RP} was inferred.

Sign and magnitude of J are indicative of the number of σ-bonds separating the π-centers of a biradical. According to the McConnell theory of exchange coupling J [29–32], the sign of J alternates with the number of σ-bonds. A single bond gives antiferromagnetic coupling ($J<0$), and two bonds give ferromagnetic coupling ($J>0$). The dipolar *through-space* contribution to J depends on the distance between the radicals and their relative orientation.

In the biradical units IIa and IIb, the second nitroxide label is linked to the fullerene in exactly the same way as the monoradical units Ia and Ib. This symmetry allows to assume that the same interaction (dipolar and exchange) between the nitroxide group and the photoexcited fullerene exists in the monoradical and biradical systems. Therefore, a strong coupling between the nitroxide spins and the fullerene triplet is expected in IIa, and a weaker one in IIb. Finally, we want to emphasize that the understanding of sign and magnitude of the exchange interaction between triplet-excited fullerenes and nitroxide radicals has been greatly advanced by the Corvaja group.

2.2 Examples from Berlin/Mülheim: High-Field EPR, EDNMR and ENDOR on Nitroxide–Solvent Interactions and Spin-Labeled Photosynthetic Reaction Centers

The inherent limitation of EPR—the need for *paramagnetic* samples—is not a serious restriction in biomolecular spectroscopy since during the last decades chemical techniques have been developed to site-specifically introduce nitroxide spin labels into diamagnetic protein molecules as “spy probes” to explore local structures and

dynamics. They allow EPR studies of the target molecules without significantly disturbing their structure and function.

Wayne Hubbel at UCLA (USA) deserves credit for being the first to have realized the potential of site-directed spin labeling (SDSL) for the exploration of protein structure and dynamics [8, 9, 33–35]. A commonly used nitroxide spin label is MTSSL (1-Oxyl-2,2,5,5-tetramethyl-3-pyrroline-3-methyl) methanethiosulfonate. MTSSL (or MTSL) is clearly the current "work-horse" and best-characterized nitroxide spin label for protein labeling [36]. W.L. Hubbell's laboratory and those of his early and later collaborators, e.g., H.-J. Steinhoff (University of Osnabrück), systematically developed the SDSL technology into a quantitative tool for structural biology that complements NMR and crystallographic methods, see for instance Refs. [37–43], and for a more recent literature review, Ref. [44].

The investigation of nitroxide spin-labeled membrane proteins using high-field EPR, ENDOR, PELDOR, EDNMR, in conjunction with quantum chemical calculations, has a long tradition in our laboratories, dating back to the early 2000s [43, 45]. The membrane protein complexes studied include bacteriorhodopsin, DNA-photolyase, colicin A toxin, bacterial photosynthetic reaction centers with particular emphasis on H-bond networks and weak solvent interactions with the cofactors. Because of the large number of protein complexes and their solvent matrices, it was not easy for us to select examples that would match both scope and spirit of our mini-review. We have decided to limit ourselves to a few interesting examples taken from Refs. [46–52].

2.2.1 Nitroxide Spin Labels Probing Hydrogen-Bond Formation

Using high-field EPR techniques either in cw or in pulsed mode of operation, the nitroxide spin-label approach has been successfully applied to various membrane and water-soluble proteins [40, 42]. The variation of the EPR parameters from site to site of the attached spin label was generally interpreted in terms of local polarity and/or hydrogen-bonding effects of the matrix [53–55].

The precision measurement of nitroxide magnetic interaction parameters provides encoded local information on solvent properties such as polarity (defined by the dielectric constant ε) and proticity (defined as propensity for hydrogen-bond formation). The appropriate interaction parameters are the g-tensor (reflecting the Zeeman and spin–orbit interactions of the unpaired electron spin), the nitrogen hyperfine A-tensor (reflecting the interaction of the unpaired electron with a ^{14}N ($I=1$) or ^{15}N ($I=1/2$) nuclear-spin), and the nitrogen quadrupole P-tensor (reflecting the interaction of the ^{14}N nuclear quadrupole moment with the electric field gradient of the electrons at this site).

In liquid solution, rapid Brownian motion averages out all anisotropic interactions and only isotropic interaction parameters are retained. Characteristic variations of A_{iso} and g_{iso} (given by 1/3 trace of the A- and g-tensors) for nitroxide radicals in solvents of different polarity and proticity were recognized already many years ago [56–59]. Shifts of g_{iso} to smaller values and A_{iso} to larger values were observed with increasing polarity of the environment. A linear correlation between $(\varepsilon-1)/(\varepsilon+1)$ and A_{iso} could be obtained for aprotic solvents [57]. Interestingly, this correlation did

not apply to protic solvents. In aprotic and protic solvents of comparable dielectric constant, larger A_{iso} shifts were observed in the protic solvent. This suggested two main effects to be responsible for the shifts: (a) non-site-specific interactions due to the bulk electric field and (b) site-specific interactions, mostly due to hydrogen bonds (H bonds), which result in local electric field changes affecting the radical's electronic structure.

Hence, the information obtained from liquid-solution magnetic resonance studies is rather limited, i.e., a detailed data interpretation requires both the value and orientation of the interaction tensors to be known. Hence, for frozen-solution matrices, the characteristics of the microenvironment are best determined by high-field/high-frequency EPR below the glass-transition temperature of the solvent. Cw EPR at high magnetic fields allows one to resolve the nitroxide *g*-tensor principal components. The g_{xx} component is particularly sensitive to the microenvironment. In addition, high-field ENDOR or ELDOR-detected NMR (EDNMR) can favorably be used to measure the nitrogen hyperfine-tensor and quadrupole-tensor components with high precision, e.g., A_{zz} and P_{zz}, which react most sensitively on interactions with the environment.

We noticed [46] that for nitroxide radicals in frozen (protic) 2-propanol, a pronounced heterogeneity of both g_{xx} and A_{zz} is present that can be resolved by W-band cw EPR and EDNMR techniques. The distinct correlation of g_{xx} versus A_{zz} values senses different nitroxide populations that are characterized by their different local environments. They were ascribed to a different hydrogen-bond network of the nitroxides, i.e., whether they develop one or two H bonds to the solvent molecules—or no H bonds at all. In a subsequent study utilizing 275 GHz cw EPR and W-band EDNMR [55], it was demonstrated that also in frozen water solution, similar to 2-propanol, two nitroxide fractions are observed. They were ascribed to nitroxide populations carrying one or two H bonds to the matrix.

Apparently, for nitroxide radicals in frozen solution, the relationship between the magnetic parameters and the hydrogen-bonding situation of the spin probe depends on the solvent matrix and is often more complex than assumed using simple models. SDSL methodology with nitroxide radicals thus requires differentiation between polarity and hydrogen bonding of the microenvironment to obtain meaningful interpretations of the experimental EPR results. Both contributions, however, are theoretically expected to affect the nitroxide magnetic parameters in a similar way. This aggravates distinction between hydrogen bonding and other non-site-specific solute–solvent interactions.

For nitroxide radicals in their solution shells, *absolute* values of the magnetic interaction tensors are still rather elaborate and problematic to calculate, e.g., by DFT methods. This is due to the solvation-dependent structure of nitroxide labels [60, 61]. The situation is different for planar quinone anion radicals in solution [62, 63]. For them excellent agreement between DFT calculations of magnetic interaction parameters and experimental values could be achieved because of good geometry data and sufficiently large solvent shell models.

To shed further light on the problem, we have investigated protic organic solvents that represent the most abundant H-bond donor groups of amino-acid side chains in proteins. In addition, we chose an aprotic and apolar solvent, *ortho*-terphenyl

Scheme 2 Structure of the two nitroxides R1 and R2 described in this work

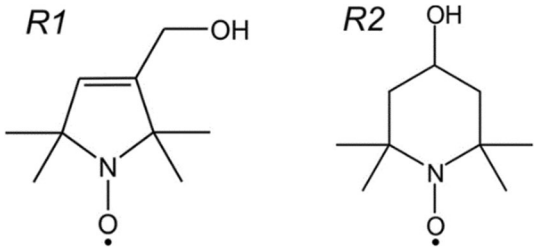

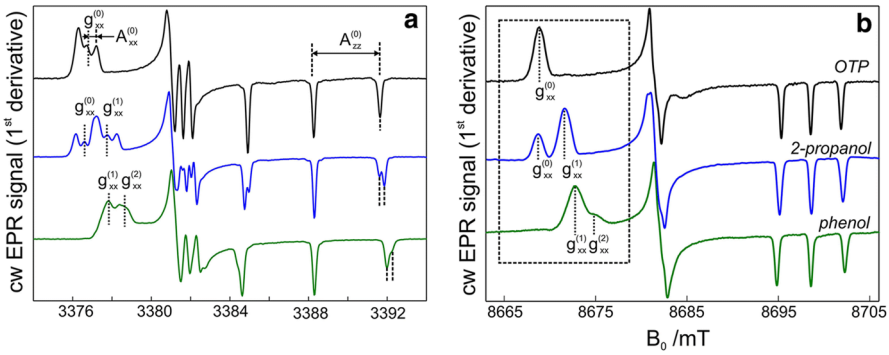

Fig. 10 Experimental **a** W-band (95 GHz) and **b** 244 GHz cw EPR spectra of nitroxide radical R1-D_{16} (Scheme 2) in frozen solutions of *ortho*-terphenyl (OTP), 2-propanol and phenol recorded at 90 K and 70 K, respectively. The spectral positions that correspond to different principal g_{xx}-tensor values and ^{14}N A_{zz} values are indicated by dotted and dashed lines, respectively (adapted from Ref. [50])

(OTP). To maximize the EPR spectral resolution, we used a perdeuterated nitroxide radical and perdeuterated solvents. The aim was to obtain reliable correlations of nitroxide magnetic parameters with the prevailing H-bond situation and the bulk solvent polarity. Since the investigated pyrroline-type nitroxide radical (3-hydroxymethyl-2,2,5,5-tetramethylpyrrolin-1-oxyl) represents the head group of the widely used MTS spin label, (S-(2,2,5,5-tetramethyl-2,5-dihydro-1H-pyrrol-3-yl)methyl-methanesulfonothioate). This information is particularly relevant for SDSL studies of spin-labeled proteins.

In our first example, we present a detailed high-field EPR investigation of magnetic parameters of the deuterated nitroxide radical R1 (see Scheme 2) dissolved in deuterated frozen solvents of polar or apolar, protic or aprotic character. The solvents include *ortho*-terphenyl, methanol, propanol, glycerol, aniline, phenol, and water (see Figs. 10 and 11). The analysis of the highly resolved 95 GHz EDNMR and 244 GHz cw EPR spectra is detailed below. This yielded precise electron Zeeman (g_{xx}), ^{14}N hyperfine (A_{zz}) and ^{14}N quadrupole (P_{zz}) tensor components. Remarkable changes in the solvation networks were found in the different matrices. The experimental data were discussed on the basis of previous semi-empirical and DFT quantum chemical calculations in an attempt to adequately model the nitroxide-matrix interactions [50]. The obtained results demonstrate that the principal values of all the magnetic interaction parameters primarily depend on the nitroxide

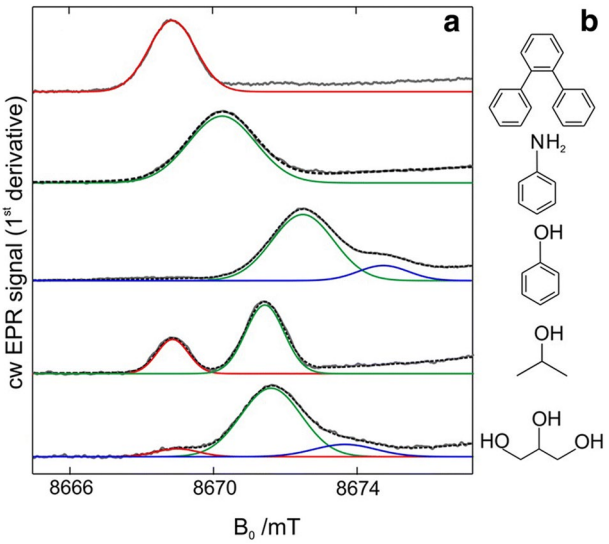

Fig. 11 **a** Comparison of the g_{xx} region of the 244 GHz cw EPR spectra of nitroxide radical R1-D_{16} in frozen solutions of (from top to bottom) OTP, aniline, phenol, 2-propanol and glycerol. The spectra were recorded at 70 K. Best-fit simulations of the line(s) are shown for zero (red), one (green) and two (blue) H bonds to the nitroxide. The spectral range presented is indicated by the dotted box in Fig. 10b. **b** Molecular structures of solvent molecules used as hosts for the diluted nitroxide solutions (adapted from Ref. [50])

hydrogen-bond situation that depends on the donor group of the solvent. The solvent bulk polarity, as described by the static dielectric constant, is of minor importance.

In Fig. 10b, the 244 GHz EPR spectra of R1-D16 in 3 different solvents are shown. The analysis of the region at low field is indicative of differences in the H-bonding situations between the nitroxide and the solvent that is strongly affecting the g_{xx} value: (i) with no H bonds for OTP (0), (ii) an equilibrium of nitroxides with one (1) and zero (0) H bonds for 2-propanol and (iii) with one (1) and two (2) H bonds in case of phenol as solvent. This is expressed in the drastic shift of the g_{xx} value of the nitroxide; examples including further solvent matrices are shown in Fig. 11. In the 244 GHz EPR spectra (Fig. 10b), the different nitrogen A_{zz} components (also A_{yy} and A_{xx}) of the nitroxide are not well resolved due to the large linewidths; these splittings can be better observed at W-band EPR (95 GHz), see Fig. 10a, and are fully resolved in the W-band EDNMR spectra shown in Fig. 12, also the ^{14}N quadrupole components P_{zz} are resolved. The employment of a ^{15}N labeled nitroxide with $I = 1/2$ lacks the quadrupole splitting and helped to precisely determine the nitrogen quadrupole parameters. Figure 13 shows a set of EDNMR spectra in different selected solvents. The formation of zero, one or two hydrogen bonds to the nitroxide has been detected and analyzed. There is a linear correlation between the solvent-induced changes of g_{xx} and ^{14}N A_{zz} and also between A_{zz} and P_{zz} values [50]. Note that the molecular differences of the solvents can lead to (slightly) different H-bond situations which is manifested in the high-field EPR and EDNMR spectra. Hydrogen bonding is clearly the dominant interaction leading

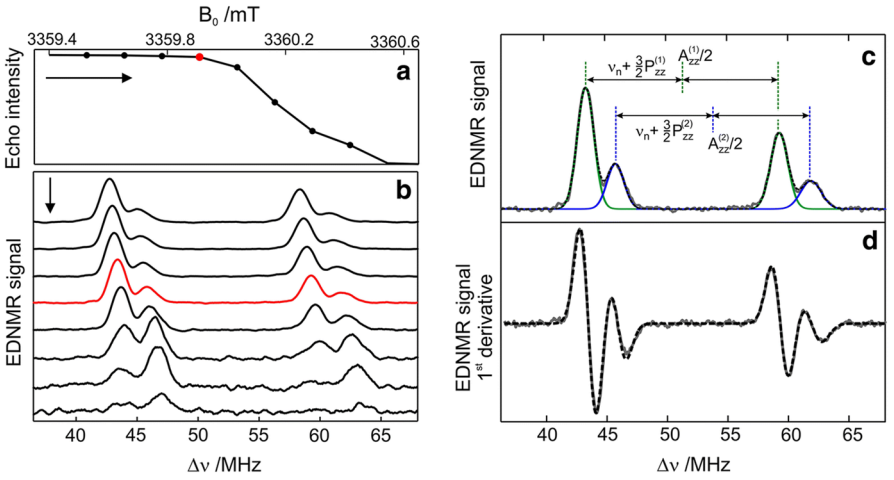

Fig. 12 W-band EDNMR spectra of R1-D_{16} in phenol-D_6 at 50 K. **a** The echo-detected EPR intensity around the g_{zz}, M_I=-1 spectral position with indicated magnetic field positions of the individual EDNMR recordings. **b** Individual ^{14}N EDNMR spectra at magnetic field positions indicated in **a**. **c** Example of two best-fit Gaussian lines to the experimental EDNMR spectrum marked in red in **b**. The two individual Gaussian components are shown by blue and green lines. **d** Experimental first-derivative EDNMR spectrum overlaid with the best-fit simulation performed in the first-derivative mode (dashed trace) (adapted from Ref. [50])

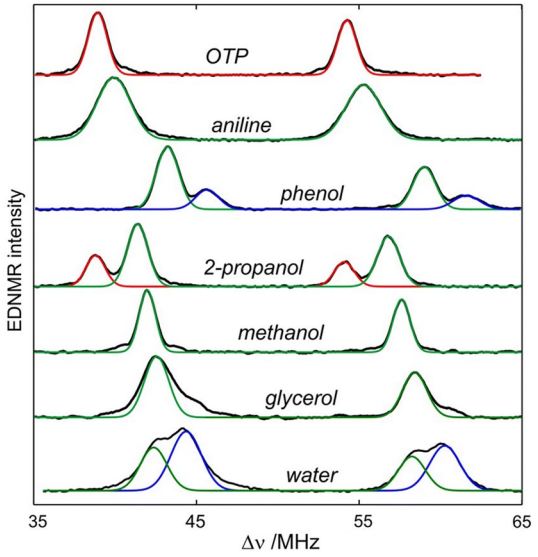

Fig. 13 W-band ^{14}N EDNMR spectra of nitroxide radical R1-D_{16} in frozen solutions of OTP, aniline, phenol, 2-propanol, methanol, glycerol and water. The spectra were recorded close to the g_{zz}, $M_I = -1$ spectral position at 50 K. The experimental spectra (black traces) are superimposed with best-fit Gaussian lines that are assigned to nitroxide radicals forming zero (red trace), one (green trace) or two (blue trace) H bonds with the solvent molecules. The EDNMR lines appear around half the ^{14}N A_{zz} hyperfine coupling (see Fig. 12c). The fits were performed on the first-derivative mode of the experimental traces; for details of the analysis, see Ref. [50] (from Ref. [50])

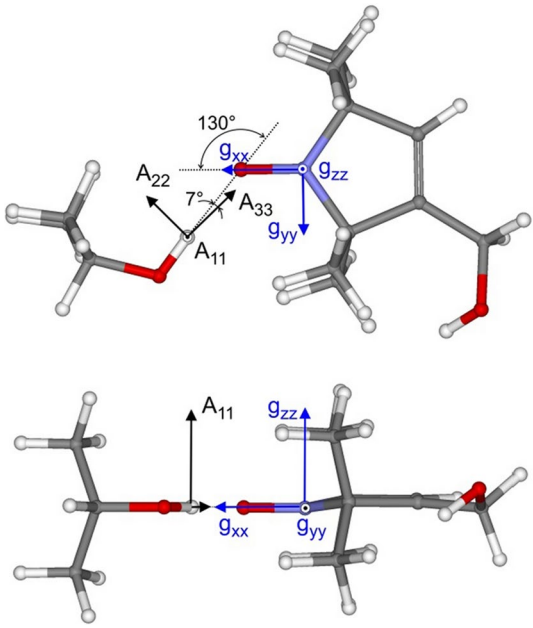

Fig. 14 Top and side views of the energy-optimized structure of the R1 nitroxide complexed with one 2-propanol molecule. The principal directions of the calculated nitroxide g- and bridged proton hyperfine tensors are indicated (from Ref. [52])

to the observed changes of the nitroxide magnetic resonance parameters; the bulk polarity of the medium plays only a minor role, as shown in Ref. [50].

Calculations show that the H bonds to R1 are preferentially formed in the molecular plane targeting the lone pairs of the oxygen of the nitroxide group carrying the electron spin (σ-type H bond). In Fig. 14, the geometry of the H-bond situation between R1 and 2-propanol is shown as an example [52]. Good agreement between the experimental and DFT-calculated spectroscopic data could be obtained. Note, however, that the H-bond situation is more complicated in case of non-planar nitroxides as demonstrated, e.g., for piperidine-type nitroxides with a six-membered ring (see R2 in Scheme 2), in which out-of-plane H bonds with (partial) π-bond character (to the oxygen and/or nitrogen) are formed [52].

An interesting aspect of EPR/ENDOR on H-bonded systems lies in the possibility to determine the hyperfine-tensor parameters of the proton (or deuteron) in the hydrogen bond. They are strongly affected by the bond length and its detailed geometry and allow an interpretation of the hydrogen bond strength affecting the physical properties of the system. Using ENDOR, this situation has been studied for nitroxide R1-D_{16} hydrogen bonded to 2-propanol-D_7(OH) glass [52]. Even more information is available from the quadrupole coupling of ^{2}H, in case the sample is prepared with a deuteron in the hydrogen bond. For more experimental details and the performed analyses, see Ref. [52]. Similar conclusions have been presented earlier for H-bonding to quinone radicals in vitro and in proteins [62–67].

We summarize: high-field EPR, ENDOR and EDNMR have been used to determine changes of the nitroxide magnetic resonance parameters caused by different solvents. Hydrogen bonding was found to play a major role in the observed changes of the NO electronic structure. NO-complexes with zero, one and two H bonds

could be observed and characterized. The planar five-membered ring system of the pyrroline-type nitroxide radical R1 was found to form well-defined in-plane σ-type hydrogen-bonded complexes with H-bond donor solvents in frozen solution. The measured hyperfine parameters of the hydrogen-bridge proton and the internal magnetic parameters describing the electron Zeeman and the electron-nuclear hyperfine and nuclear quadrupole interactions are in good agreement with values predicted by state-of-the-art DFT calculations. In contrast, multi-resonance EPR on the non-planar six-membered ring system of piperidine-type nitroxide radicals (e.g., TEMPOL, R2) reveals a more complex situation, i.e., a mixture of a σ-type and an out-of-plane π-type complex, both present in comparable fraction in frozen solution. For such systems, it is more difficult to predict magnetic interaction parameters using quantum chemical calculations, probably due to the considerable flexibility of the nitroxide and hydrogen-bonded complex. The detailed information about nitroxide/solvent complexes is of particular importance for dynamic nuclear polarization (DNP) and site-directed spin-labeling EPR studies that employ nitroxides as polarizing agents or spin labels, respectively.

2.2.2 Local Water Sensing: Water Exchange in Bacterial Photosynthetic Reaction Centers Embedded in a Trehalose Glass Studied by High-Field Multi-resonance EPR

Water plays an essential role in the chemistry of life. It governs the internal dynamics of biological macromolecules, such as proteins. Unrestricted dynamics at a specific time scale is a crucial requirement for the specific biological activity of proteins. This includes enzyme activity, macromolecular recognition, ligand binding and participation in electron and proton transfer processes for biological function. Under physiological conditions, (bio)macromolecules fluctuate between a multitude of conformational sub-states in a rugged energy landscape that is hierarchically organized in energy tiers [68–70]. Their dynamics span an enormous time range, from sub-picosecond to tens of microseconds, and include a multitude of stochastic local and collective motions, from bond vibrations to domain motions [69, 71, 72]. Water drives protein folding through hydrophobic interactions [73–76], but also contributes to the stabilization of the 3D protein structure and modulates the protein dynamics [77]. For most proteins cooled below the glass-transition temperature (typically around 200 K), their biological function is blocked due to restricted conformational motion.

In biological systems, the solvent water is generally divided into three distinctly different classes of functionality: (i) internal, strongly bound water that cannot be removed even upon lyophilization; (ii) surface water in the hydration shell of the protein at the solute–solvent interface, and (iii) bulk water randomly distributed in the protein matrix. Water molecules in the protein hydration layer have restricted dynamics compared to water molecules in the bulk. The thickness of the hydration layer at the solute–solvent interface is still a matter of debate.

The “freezing out” of conformational dynamics by lowering the temperature is a common strategy for studying function-dynamics relationships in proteins. To minimize freezing damage by ice crystals, proteins are usually frozen in the

presence of cryoprotectants. This approach is, however, problematic because it aggravates disentanglement of the influences of solvent and temperature on the protein dynamics. An elegant alternative approach is to embed the protein into amorphous matrices formed by disaccharides like trehalose (α-D-glucopyranosil-α-D-glucopyranoside) [78, 79], see Fig. 16b. This allows the native protein folding to be preserved during extensive protein dehydration, even at temperatures well above room temperature. In nature, the extraordinary bio-protective capabilities of disaccharide glasses are exploited by specific organisms, which are able to survive extreme conditions of temperature and dehydration by entering a state of reversibly arrested metabolic activity, called *anhydrobiosis* ("Life without water") [79–81].

At room temperature, the stepwise dehydration of the trehalose matrix results in increasingly inhibited dynamics of the embedded protein. This was observed in both small globular proteins like myoglobin [78, 82] and large membrane proteins like bacterial photosynthetic reaction centers [79, 83] as well as photosystem I [84] and photosystem II [85] of oxygenic photosynthesis.

Trehalose is the most efficient sugar for bio-protection against extreme dehydration and osmotic stress. It is an active stabilizer of enzymes, proteins, vaccines, pharmaceutical preparations and even organs for transplantation. The mechanistic details of trehalose efficiency are, however, not yet clear, but probably involve a combination of several factors that include its extraordinarily high glass-transition temperature (385 K) [86], its distinct propensity for hydrogen-bonding and the pronounced rigidity of its dehydrated glass matrix [87].

In the following, we wish to address the biologically important question of detection and quantification of local water, in contrast to bulk water, in membrane proteins. For water sensing, we chose the bacterial reaction center (bRC) from *Rhodobacter (Rb.) sphaeroides* R26, in which the paramagnetic Fe^{2+} had been replaced by diamagnetic Zn^{2+}. The Zn-bRC was embedded into a trehalose glass matrix [49]. Local water sensing was made possible by monitoring the electron–nuclear hyperfine interaction of isotope-enriched water (D_2O and $H_2{}^{17}O$) with the paramagnetic sites of the bRC.

The bRC of *Rb. sphaeroides* is an integral membrane protein (see Fig. 15a, b) that catalyzes the primary photochemical processes to convert light energy into chemical free energy [88–90]. The three protein subunits, L, M, and H host several cofactors [91] sequentially involved in light-driven electron transfer. Two bacteriochlorophyll *a* (BChl *a*) molecules (blue) near the periplasmic side of the membrane form the "special pair" P_{865}, the primary electron donor. After photoexcitation to its singlet state, the subsequent electron transfer proceeds predominantly via the protein branch A [88] to the Q_A acceptor. In the present study, the secondary electron-transfer step, $Q_A^{\bullet-} \rightarrow Q_B$, is blocked using the inhibitor stigmatellin [92]. Thus, in the charge separation process the radical pair state $P_{865}^{\bullet+} Q_A^{\bullet-}$ is created in very high yield with *two* radical species located in a different protein environment.

The native bRC contains five cysteine residues buried within the protein domains, with the exception of cysteine 156, which is moderately solvent-exposed in subunit H. The cysteine 156 residue can be site-specifically spin labeled with an external paramagnetic probe molecule. We used MTSSL [93, 94]. The nitroxide label in

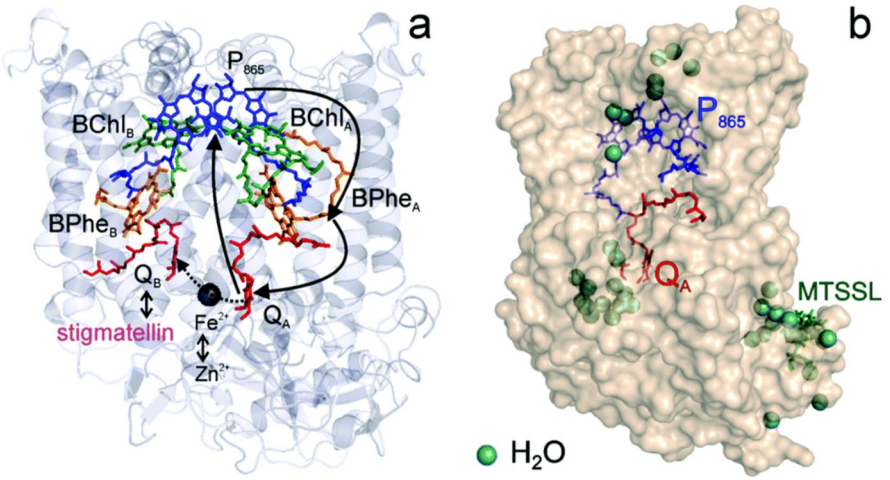

Fig. 15 **a** X-ray structural model of the bRC from *Rb. sphaeroides* R26 [112] with the protein subunits L, M, and H carrying the electron-transfer cofactors P_{865} (a bacteriochlorophyll *a* (BChl) dimer that forms the "special pair" electron donor) near the periplasmic side of the membrane, two monomeric BChl's, two BPhe's (bacteriopheophytin *a*), two ubiquinone-10 molecules (Q_A and Q_B) and a non-heme iron Fe^{2+}. The paramagnetic Fe^{2+} cofactor is replaced by diamagnetic Zn^{2+}. Q_A and Q_B form the primary and secondary electron acceptor, respectively. Light-induced electron transfer proceeds predominantly along the A branch of the cofactors ("unidirectionality" enigma). Here, the quinone Q_B is replaced by stigmatellin to block the secondary electron-transfer step from $Q_A^{\bullet-}$ to Q_B. **b** Molecular surface representation of the spin-labeled bRC (SL-bRC) from *Rb. sphaeroides* R26, indicated are the primary electron donor P_{865} (in blue), the primary electron acceptor Q_A (in red) and the nitroxide spin label MTSSL attached to Cys156 in the H protein subunit (in green). Strongly bound water molecules within 1 nm radius of each paramagnetic center are shown as greenish colored spheres, they were obtained from the a high resolution X-ray structure [113] (adopted from Ref. [49])

the bRC protein [95] provides a third paramagnetic probe within the bRC besides the "natural" radical ions $P_{865}^{\bullet+}$ and $Q_A^{\bullet-}$. The W-band EPR spectra of the 3 radicals are schematically depicted in Fig. 16a. According to the protein 3D structure, the three paramagnetic reporter groups are in distinctly different local environments (see Fig. 15b) and serve as local probes to identify water molecules via dipolar and quadrupolar hyperfine interactions with either D (^{2}H) or ^{17}O nuclei.

In bRCs, a coating with trehalose influences the lifetime of the charge-separated radical pair state, $P_{865}^{\bullet+}Q_A^{\bullet-}$. Upon progressive dehydration of the trehalose matrix, the kinetics of $P_{865}^{\bullet+}Q_A^{\bullet-}$ charge recombination becomes faster and exhibits widely distributed rate constants [79, 81, 96, 97]. Two relative hydration levels, r, were chosen in this work, which result in a different extent of slaving the protein dynamics to the embedding sugar matrix: (i) $r = 11\%$ for which the protein dynamics is arrested on the time scale of seconds [97], and (ii) $r = 74\%$ for which the dynamics is only mildly retarded as compared to solution [98]. Note that in the dehydrated (dry) case $r = 11\%$ the solution contains only ~ 0.5 waters per trehalose molecule.

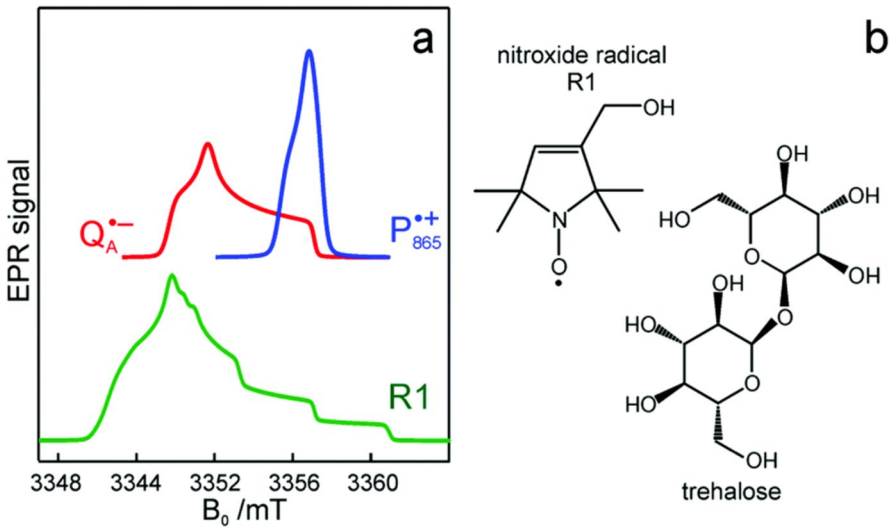

Fig. 16 **a** Simulated rigid limit W-band EPR absorption spectra of $P_{865}^{\bullet+}$ (blue trace), $Q_A^{\bullet-}$ (red trace), and of the nitroxide radical R1 (green trace). **b** Chemical structures of the pyrroline-type nitroxide radical R1 and the disaccharide trehalose (from Ref. [49])

The relative hydration levels r were adjusted by applying the isopiestic method of controlled sample dehydration [99]. It has been employed successfully both in EPR [100] and IR spectroscopy [101–103]. The samples were transferred into a sealed box where further dehydration of the sample occurred via controlled exposition to an atmosphere of low relative humidity over a saturated aqueous salt solution at room temperature using H_2O with natural isotope abundance. For measurements on samples equilibrated to the desired relative humidity with either D_2O or $H_2{}^{17}O$ vapor, the saturated solutions of an adequate salt were prepared using the respective isotope labeled water at room temperature.

In a first series of experiments, the trehalose glass was characterized after dehydration at different humidity levels using the homogeneously dispersed spin label R1 (Fig. 17b) *in absence* of the protein (bRC). The D_2O content was determined by W-band EDNMR monitoring the amplitude of the D-NMR signal associated with the nitroxide signal (at position g_{zz}, $M_I=0$), see Fig. 17. The spectra in panel **a** show the signal for the sample directly prepared in D_2O (top, red) and for a series of exchange times (6–170 h) of the sample after it had been equilibrated at $r=11\%$ ($LiCl/D_2O$). A control prepared with H_2O shows no D matrix signal. The D matrix line at the D Larmor frequency (21.9 MHz) shows a clear dependence on time depicted in panel **c**, reaching a plateau after approx. 3 days. It only reaches ~ 50% of the intensity of the sample prepared directly in D_2O. This indicates that the trehalose hydroxyl groups exchange slower and do not contribute significantly to the water exchange experiment [49]. In the range, 30–55 MHz signals from the ^{14}N of the nitroxide appear with similar intensity over the whole time range.

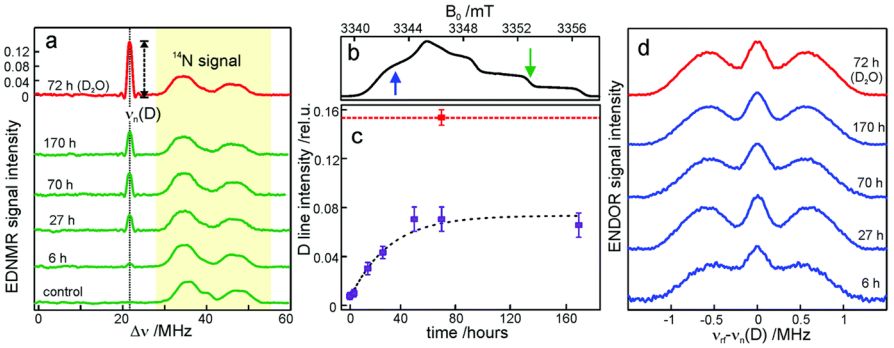

Fig. 17 **a** W-band EDNMR spectra recorded for R1/trehalose glasses at 60 K. The glasses were equilibrated with a saturated LiCl/D_2O solution for the indicated time. The red trace corresponds to the R1/trehalose glass prepared in D_2O. The spectra were recorded at the field position indicated in **b** by the green arrow. **b** Echo-detected field-swept W-band EPR spectrum of the nitroxide radical R1 embedded in trehalose glass. **c** Intensity of the deuterium EDNMR line as a function of equilibration time. The red dashed line corresponds to the deuterium line intensity evaluated for R1/trehalose glass prepared in D_2O. The error margins are determined by data analysis from two independent series of measurements. **d** W-band Mims ENDOR spectra recorded for R1/trehalose glasses at 60 K. The glasses were equilibrated with a saturated LiCl/D_2O solution for the indicated time. The red trace corresponds to R1/trehalose glass prepared directly in D_2O. The spectra were recorded at the field position indicated in **b** by the blue arrow (adopted from Ref. [49])

The "matrix line" detected at ν_D could be simulated with a Gaussian lineshape for all spectra, no sign of splitting or shoulders were observed. No D nuclei hyperfine coupled to the nitroxide could be detected, which are expected for H bonds to the NO group. To check on this interaction, a series of Mims ENDOR spectra were measured in the g_{xx}–g_{yy} range where the largest D ENDOR couplings were expected (see Fig. 17d). Here, after 6 h of exchange a D hyperfine splitting of 1.8 ± 0.3 MHz was observed, in addition to the matrix line. Thus, both *distant* and *local* (H bonded) deuterium signals could be detected. However, the linewidth is rather broad in the rigid dry trehalose glass preventing detection of accurate hyperfine and nuclear quadrupole interactions. A much better resolution was observed in case of rehydration of trehalose at $r = 74\%$ where the nitroxide molecules are expected to sit predominantly in water-rich domains that allow an optimum geometry of the nitroxide–hydrogen bond complexes to be formed (see Fig. S3 and S5 in Ref. [49]). Here, an increasing fraction of nitroxides is forming not only one but two H bonds to the solvent.

This series of experiments performed on the nitroxide R1/trehalose system shows how water sensing can be performed using labeled water (D_2O) in combination with high-field EPR and EDNMR/ENDOR. It also demonstrates how directly coordinated (e.g., H bonded) and distant water can be distinguished. This approach has also been used in exactly the same way to study spin-labeled proteins, e.g., the Zn-substituted bRC introduced above (see Fig. 4a-b in Ref. [49]). In this work, we noticed that other protons at the protein could undergo H/D exchange and add intensity to the D matrix line leading to complications in the analysis. In such cases it is advantageous to use $H_2{}^{17}O$, i.e., ^{17}O as nuclear spin probe as is demonstrated below.

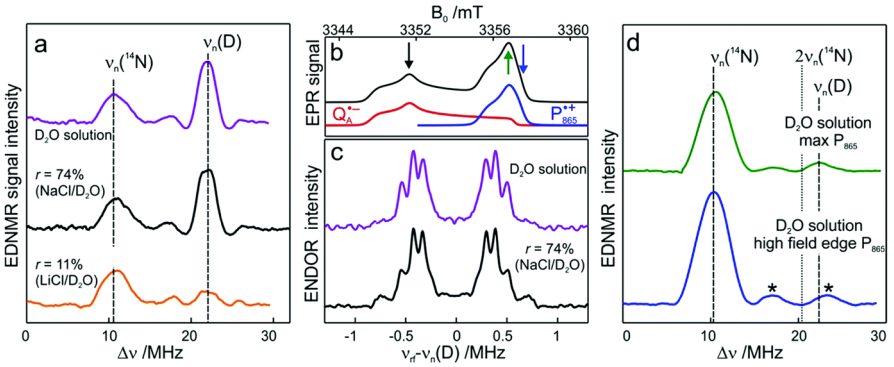

Fig. 18 **a** W-band EDNMR spectra recorded at the field position of maximum signal intensity of the $Q_A^{\bullet-}$ EPR spectrum (marked by the black arrow in **b**). **b** The sum of EPR absorption spectra of $P_{865}^{\bullet+}$ and $Q_A^{\bullet-}$ ionic states of cofactors (black trace). The simulated spectra corresponding to $Q_A^{\bullet-}$ (red trace) and $P_{865}^{\bullet+}$ (blue trace) are also shown. **c** W-band ENDOR spectra for bRCs in solution dissolved in Tris/HCl buffer prepared in D_2O, and for bRC/trehalose glass equilibrated at $r=74\%$ ($NaCl/D_2O$) recorded at the field position indicated by the black arrow in (b) for $Q_A^{\bullet-}$. **d** W-band EDNMR spectra for bRCs dissolved in Tris/HCl buffer prepared in D_2O recorded at field positions indicated by green and blue arrows in **b** for $P_{865}^{\bullet+}$. For details, see Ref. [49] (adopted from Ref. [49])

In the Zn-bRC, two additional paramagnetic centers $P_{865}^{\bullet+}$ and $Q_A^{\bullet-}$ are present under illumination and can be used for water sensing in the surrounding of the radicals in the protein (see Fig. 18). For $Q_A^{\bullet-}$(Fig. 18a), W-band EDNMR detects an (unsplit) ^{14}N resonance in all spectra that is assigned to nitrogen(s) from His(M219) and/or Ala(M260), i.e., from residues known to be involved in formation of tight hydrogen bonds to the oxygens of $Q_A^{\bullet-}$[63–67]. At the D Larmor frequency ν_D, a deuterium matrix line is observed, its intensity is approximately the same in frozen D_2O and Zn-bRC/trehalose rehydrated at $r=74\%$ ($NaCl/D_2O$). This shows that the diffusion of water within the protein in rehydrated trehalose is not hampered as compared to that of protein in solution. In case of the dry protein/trehalose glass ($r=11\%$, $LiCl/D_2O$) the D matrix line is also present but is only 1/10 of that in frozen solution. Clearly, trehalose coating does not prevent water exchange, which happens between trehalose and protein on the same time scale as between trehalose and the vapor atmosphere [49].

The large linewidth prevents resolution of the D hfcs in the EDNMR. In Fig. 18c, D ENDOR spectra are shown for Zn-bRCs/trehalose ($r=74\%$ rehydration) and in buffer/D_2O solution. The spectra are identical and could be analyzed, and they result from D in hydrogen bonds to $Q_A^{\bullet-}$ in well-defined geometry with dipolar and quadrupolar contributions. These have been observed and analyzed earlier [63–67]. It should be noted that embedding in a trehalose matrix is not changing the H-bonding geometry to the quinone that is important for the function of the ET in the bRC.

Water exchange in the surrounding of $P_{865}^{\bullet+}$ could also be probed by selecting a position for EDNMR and ENDOR in the W-band EPR where only $P_{865}^{\bullet+}$ absorbs (see Fig. 18b). In the EDNMR spectrum, strong ^{14}N resonances from the BChl *a* molecules in $P_{865}^{\bullet+}$ are observed at the $\nu(^{14}N)$ Larmor frequency. In addition, the respective

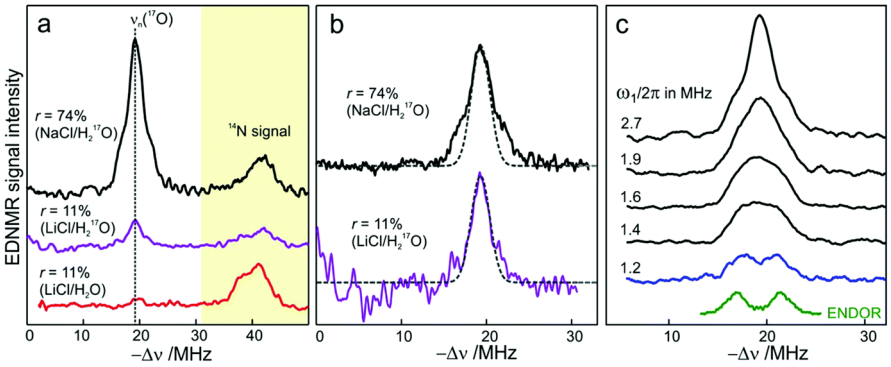

Fig. 19 **a** W-band EDNMR spectra for SL-bRC/trehalose glass samples equilibrated for 70 h at $r=74\%$ ($NaCl/H_2{}^{17}O$) black trace; $r=11\%$ ($LiCl/H_2{}^{17}O$) magenta trace; and $r=11\%$ ($LiCl/H_2O$) red trace. The spectra were recorded at the same nitroxide spectral position (g_{zz}, $M_I=0$) indicated in Fig. 14b by the green arrow. EDNMR spectra are shown for $\nu<0$ to obtain a better separation between ^{17}O and ^{14}N signal contributions (see Fig. S2b in SI of ref. [49]). **b** The ^{17}O EDNMR spectra for $r=74\%$ ($NaCl/H_2{}^{17}O$) (black trace) and $r=11\%$ ($LiCl/H_2{}^{17}O$) (magenta trace) samples. The gray dashed lines show the best-fit simulation of experimental recordings to a Gaussian line. **c** Microwave field amplitude dependence of ^{17}O EDNMR spectra of SL-bRC/trehalose glasses equilibrated for 3 days at $r=11\%$ ($LiCl/H_2{}^{17}O$). The black spectra were recorded using an HTA pulse length of $t_{HTA}=20$ µs. The blue trace shows the EDNMR spectrum acquired with $t_{HTA}=7$ µs. The green line shows the Davies ENDOR spectrum recorded at the same spectral position (from Ref. [49])

double-quantum transitions are detected which overlap with the D matrix signal at 21.8 MHz. The lack of a (detectable) D matrix line is possibly due to the absence of exchangeable water in the vicinity of $P_{865}^{\bullet+}$; however, this conclusion needs further confirmation. The delocalized spin density distribution over the large $P_{865}^{\bullet+}$ dimer could be the reason for the absence of D hfcs large enough for detection [104]. This is, however, not the case for liquid-solution ENDOR of $P_{865}^{\bullet+}$ [105, 106] or the related BChl *a* radical cation [107].

In the last example, ^{17}O is used as nuclear-spin probe instead of D, i.e., $H_2{}^{17}O$ water is employed. This is necessary since with D_2O unwanted H/D exchange could take place in the water sensing experiments preventing quantitative conclusions. In Fig. 19, ^{17}O EDNMR experiments are shown on spin-labeled bRC/trehalose equilibrated at $r=11\%$ ($LiCl/H_2{}^{17}O$) and at $r=74\%$ ($NaCl/H_2{}^{17}O$) with the magnetic field positioned at the NO spin label (g_{zz}, $M_I=0$). In both spectra, a resonance at the ^{17}O Larmor frequency is present at 19.4 MHz as well as ^{14}N lines from the nitroxide nitrogen. At low hydration level ($r=11\%$), the ^{17}O matrix line is ~6 times smaller than at the high hydration level ($r=74\%$). Here, the difference in water content is more pronounced as in the case of D_2O, where H/D exchange contributes to the D line intensity. Based on the lineshape, the water molecules are assumed to belong to distant waters in the "dry case", whereas at higher hydration levels also, local water molecules contribute that are hyperfine-coupled to the nitroxide. This is seen from the spectra presented in Fig. 19b, showing clear wings for the hydrated sample. In Fig. 19c, we have tried to improve the resolution of the coupled ^{17}O nuclei and distinguish them from distant nuclei by changing the mw field and HTA pulse

amplitude [108] in the EDNMR spectra (blue trace). For comparison, a Davies ENDOR spectrum (green) is also shown in which the matrix line is suppressed. The latter ^{17}O EDNMR and ENDOR experiments clearly show a direct bonding of the water to the nitroxide probably via hydrogen bonding. This forms a promising basis for further experiments using these techniques in combination with ^{17}O labeled water.

Finally, we note that recently there appeared a publication by the group of M. Bennati (Göttingen, Germany) about ^{17}O hyperfine spectroscopy of the hydration structure of nitroxide radicals in aqueous solutions with support of quantum chemical calculations and MD simulations [109].

Conclusions: In the presented work, water accessibility was measured at 3 different sites within a membrane protein, the bRC of *Rb. sphaeroides*. The paramagnetic reporter groups have distinctly different surroundings in the protein and can probe different types of water, i.e., internal, bulk and surface water. The bRC was embedded in a trehalose matrix and equilibrated at low ($r = 11\%$) and high ($r = 74\%$) relative humidity. At low humidity, the matrix is rigid (with only ~ 0.5 waters per sugar molecule), whereas at higher humidity, more water molecules can serve as solvation partners for the protein.

To obtain details of the related hydration/dehydration process, the bRC/trehalose system was studied by sensitive high-resolution techniques, namely high-field EPR, EDNMR and ENDOR. The results show that these methods are very well suited to detect water in the vicinity of radical sites in the protein via dipolar and quadrupolar hyperfine interactions of magnetic nuclei such as D or ^{17}O when, respectively, labeled water (D_2O and $H_2{}^{17}O$) is used for water exchange. The use of (the rather expensive) $H_2{}^{17}O$ has the advantage to avoid H/D exchange of the protein and should thus be used for quantitative studies.

The detailed analysis of the data demonstrated the very high efficacy of the trehalose in bio-protection. Several of the various models existing in the literature trying to explain the special impact of this sugar on proteins, could be excluded based on the obtained results (for a detailed discussion, see Ref. [49]. It could further be shown that the best approach to explain hindering of the protein dynamics is provided by the "anchorage model" [110], in which a tight anchoring of the protein surface to the rigid matrix by an extended H-bond network is proposed.

The obtained spectra show that water molecules, detectable by the NO spin label attached to the bRC surface, are retained in the first and second solvation shell, even under extensive drying conditions ($r = 11\%$) that block the internal protein dynamics. Experiments on an intrinsic spin probe ($Q_A^{\bullet -}$) in the bRC showed that residual protein motion still allows for exchange of strongly bound water within the protein and H/D exchange near the quinone radical site. The hydrogen bonding to the acceptor quinones has been discussed as key factor for proton-coupled electron transfer (PCET) and for the functioning of the bRC [111].

Our preliminary experiments using W-band ^{17}O EDNMR and ENDOR gave very promising results: the ratio of the matrix ^{17}O line at low and high humidity levels mirrored the water/trehalose molar ratio of both hydration states. Furthermore, detection of the ^{17}O hyperfine coupling at higher hydration levels could be

accomplished. Future work along these lines promises to deliver exquisite details of the water–protein interaction.

The presented methodology, W-band ^{17}O EDNMR and ENDOR in conjunction with ^{17}O isotope labeled water is very well suited for local water sensing in bio-macromolecules. Clearly, a key issue is the understanding of the different types of water in living matter. It has been recognized that water is far more than merely a simple solvent—it is also indispensable for biological function.

Epilogue

We return to the *Prologue*, which dealt with our first encounter with Carlo Corvaja. That was in 1965 during the International EPR Conference in Cirencester. Despite the Iron Curtain in Europe, there were still possibilities to meet EPR colleagues from West and East, in rare cases even from the USSR. A quarter of a century later, the Iron Curtain got pretty big holes, and East–West get-togethers became more frequent. New promising opportunities for East–West scientific cooperations opened up. Like all of us, Carlo Corvaja was also enthusiastic about these new opportunities and determined to seize them for the benefit of both sides. An outstanding example was the close collaboration with Yakov S. Lebedev and his team at the Institute of Chemical Physics of the Academy of Sciences in Moscow. It started in the early 1990s and lasted until his much too early death in 1996. During these years, Carlo Corvaja met Yakov Lebedev and his coworker Alexander Dubinskii as well as Yuri Grishin from Novosibirsk while visiting our high-field EPR laboratory in Berlin.

In these years of thaw between East and West, generous public research funding programs were launched, e.g., by the German Research Foundation (DFG) the Priority Area "High-Field EPR Spectroscopy". The EPR groups in Padova, Moscow, Novosibirsk, Kazan and Rehovot (Israel) were also involved in this Priority Area, whose scientists benefited greatly from the new exchange options with the EPR laboratories in Berlin and Mülheim. In addition, indeed, we have now been fortunate to meet with Carlo Corvaja at new conference venues, e.g., in Venice, Padova, Kazan and Novosibirsk.

One man was on everyone's lips at the time who had made this possible on the part of the Soviet Union: Mikhail Gorbachev (Gorbatschow), General Secretary of the Communist Party of the USSR. "Glasnost" and "Perestroika" describe the direction of his reforms. This development also benefited the foundation of "Applied Magnetic Resonance" in Kazan, the first international scientific journal in the USSR that published articles exclusively in English. Interestingly, since 1990 advertising posters with the name Gorbatschow appeared all over Berlin, on buses, trains and buildings. In fact, they were advertising the Gorbatschow vodka brand, which had been founded in Berlin already in 1921. In a delightful ambiguity, sales of Gorbatschow vodka increased rapidly.

At present, political, economic and cultural relations between East and West have drastically deteriorated again. We do hope that the political decision-makers will be guided in the near future by the spirit of peace.

The authors of this article can only add: "*Dum spiro spero*", which translates to "As long as I breathe, I hope".

Acknowledgements We thank all our collaborators of the work described in this mini-review for their valuable contributions. They are acknowledged in the original articles cited here. This work is supported by the Deutsche Forschungsgemeinschaft and the Max-Planck-Gesellschaft. K. M. and M. P. acknowledge sustaining support by the Freie Universität Berlin.

Author Contributions K.M., A.S., M.P. and W.L. wrote the manuscript. All the authors reviewed the manuscript.

Funding Open Access funding enabled and organized by Projekt DEAL.

Data Availability No datasets were generated or analyzed during the current study.

Declarations

Conflict of interest The authors declare no competing interests.

References

1. E. McMullin (ed.), *Galileo: Man of Science* (Basic books, New York, 1967)
2. D. Carbonera, M. Di Valentin, C. Corvaja, G. Giacometti, G. Agostini, P.A. Liddell, A.L. Moore, T.A. Moore, D. Gust, J. Photochem. Photobiol. C. **105**, 329–335 (1997)
3. D. Carbonera, M. Di Valentin, C. Corvaja, G. Agostini, G. Giacometti, P.A. Liddell, D. Kuciauskas, A.L. Moore, T.A. Moore, D. Gust, J. Am. Chem. Soc. **120**, 4398–4405 (1998)
4. M. Huber, H. Kurreck, B. von Maltzan, M. Plato, K. Möbius, J. Chem. Soc. Faraday Trans. **86**, 1087–1094 (1990)
5. D. Stehlik, K. Möbius, Annu. Rev. Phys. Chem. **48**, 745–784 (1997)
6. H. Levanon, K. Möbius, Annu. Rev. Biophys. Biomol. Struct. **26**, 495–540 (1997)
7. C. Corvaja, A. Toffoletti, F. Conti, M. Maggini, G. Scorrano, Time-resolved EPR of C_{60} derivatives in photoexcited triplet and quartet states, in *Recent Advances in Chemistry and Physics of Fullerenes and Related Materials*, vol. 5, ed. by K.M. Kadish, R.S. Ruoff (The Electrochemical Society, Pennington, 1997), pp.213–224
8. L.J. Berliner (ed.), *Spin Labeling Theory and Applications*, vol. I (Academic Press, New York, 1976)
9. L.J. Berliner (ed.), *Spin Labeling Theory and Applications*, vol. II (Academic Press, New York, 1979)
10. N. Mizuochi, Y. Ohba, S. Yamauchi, J. Phys. Chem. A **101**, 5966–5968 (1997)
11. N. Mizuochi, Y. Ohba, S. Yamauchi, J. Phys. Chem. A **103**, 7749–7752 (1999)
12. M. Mazzoni, F. Conti, C. Corvaja, Appl. Magn. Reson. **18**, 351–361 (2000)
13. F. Conti, C. Corvaja, A. Toffoletti, N. Mizuochi, Y. Ohba, S. Yamauchi, M. Maggini, J. Phys. Chem. A **104**, 4962–4967 (2000)
14. L. Franco, M. Mazzoni, C. Corvaja, V.P. Gubskaya, L.S. Berezhnaya, I.A. Nuretdinov, Mol. Phys. **104**, 1543–1550 (2006)
15. D.M. Guldi, N. Martin (eds.), *Synthesis of Methanofullerenes for Materials Science and Biological Applications* (Springer, Dordrecht, 2002)

16. G. Possamai, S. Marcuz, M. Maggini, E. Menna, L. Franco, M. Ruzzi, S. Ceola, C. Corvaja, G. Ridolfi, A. Geri, N. Camaioni, D.M. Guldi, R. Sens, T. Gessner, Chem. Eur. J. **11**, 5765–5776 (2005)
17. M. M. Haugland, E. A. Anderson and J. E. Lovett, Tuning the properties of nitroxide spin labels for use in electron paramagnetic resonance spectroscopy through chemical modification of the nitroxide framework. *in Electron Paramagnetic Resonance, Vol 25* (Chechik, V. and D. M. Murphy, eds.), (2017), pp. 1–34
18. C. Corvaja, M. Maggini, M. Prato, G. Scorrano, M. Venzin, J. Am. Chem. Soc. **117**, 8857–8858 (1995)
19. C. Corvaja, L. Franco, M. Mazzoni, Appl. Magn. Reson. **20**, 71–83 (2001)
20. L. Franco, M. Mazzoni, C. Corvaja, V.P. Gubskaya, L.S. Berezhnaya, I.A. Nuretdinov, Chem. Commun. (2005). https://doi.org/10.1039/b417056c
21. M. Prato, M. Maggini, G. Scorrano, Synth. Met. **77**, 89–91 (1996)
22. L. Franco, M. Mazzoni, C. Corvaja, V.P. Gubskaya, L.S. Berezhnaya, I.A. Nuretdinov, Appl. Magn. Reson. **30**, 577–590 (2006)
23. C.D. Buckley, K.A. McLauchlan, Mol. Phys. **54**, 1–22 (1985)
24. C. Blattler, F. Jent, H. Paul, Chem. Phys. Lett. **166**, 375–380 (1990)
25. N.I. Avdievich, M.D.E. Forbes, J. Phys. Chem. **99**, 9660–9667 (1995)
26. Y. Kobori, K. Takeda, K. Tsuji, A. Kawai, K. Obi, J. Phys. Chem. A **102**, 5160–5170 (1998)
27. K.M. Salikhov, Y.N. Molin, R.Z. Sagdeev, A.L. Buchachenko, *Spin Polarization and Magnetic Effects in Radical Reactions* (Elsevier, Amsterdam, 1984)
28. L.T. Muus, P.W. Atkins, K.A. McLauchlan, J.B. Pedersen (eds.), *Chemically Induced Magnetic Polarization* (Springer, Dordrecht, 1977)
29. H.M. McConnell, J. Chem. Phys. **33**, 115–121 (1960)
30. H.M. McConnell, A.D. McLachlan, J. Chem. Phys. **34**, 1–000 (1961)
31. C. Kollmar, O. Kahn, J. Am. Chem. Soc. **113**, 7987–7994 (1991)
32. H.M. McConnell, Proc. R. A. Welch Found. Chem. Res. **11**, 144–154 (1967)
33. H.M. McConnell, W.L. Hubbell, J. Am. Chem. Soc. **93**, 314–326 (1971)
34. K. Hong, W.L. Hubbell, Proc. Natl. Acad. Sci. U.S.A. **69**, 2617–2621 (1972)
35. W.L. Hubbell, C. Altenbach, Site-directed spin labeling of membrane proteins, in *Membrane Protein Structure: Experimental Approaches*. ed. by S.H. White (Springer, New York, 1994), pp.224–248
36. K. Ackermann, A. Chapman, B.E. Bode, Molecules **26**, 7534 (2021)
37. M.R. Fleissner, D. Cascio, W.L. Hubbell, Protein Sci. **18**, 893–908 (2009)
38. H.S. McHaourab, M.A. Lietzow, K. Hideg, W.L. Hubbell, Biochemistry **35**, 7692–7704 (1996)
39. D.T. Warshaviak, L. Serbulea, K.N. Houk, W.L. Hubbell, J. Phys. Chem. B **115**, 397–405 (2011)
40. H.J. Steinhoff, A. Savitsky, C. Wegener, M. Pfeiffer, M. Plato, K. Möbius, Biochim. Biophys. Acta **1457**, 253–262 (2000)
41. C. Wegener, A. Savitsky, M. Pfeiffer, K. Möbius, H.J. Steinhoff, Appl. Magn. Reson. **21**, 441–452 (2001)
42. E. Bordignon, H. Brutlach, L. Urban, K. Hideg, A. Savitsky, A. Schnegg, P. Gast, M. Engelhard, E.J.J. Groenen, K. Möbius, H.J. Steinhoff, Appl. Magn. Reson. **37**, 391–403 (2010)
43. Möbius, A. Savitsky, *High-Field EPR Spectroscopy on Proteins and their Model Systems* (RSC Publishing, Cambridge, 2009)
44. F. Torricella, A. Pierro, E. Mileo, V. Belle, A. Bonucci, Biochim. Biophys. Acta Proteins Proteom. **1869**(7), 140653 (2021)
45. K. Möbius, W. Lubitz, A. Savitsky, High-field EPR in membrane proteins—crossing the gap to NMR. Progr. NMR Spectrosc. **75**, 1–49 (2013)
46. A. Nalepa, K. Möbius, W. Lubitz, A. Savitsky, J. Magn. Reson. **242**, 203–213 (2014)
47. K. Möbius, A. Savitsky, A. Nalepa, M. Malferrari, F. Francia, W. Lubitz, G. Venturoli, Appl. Magn. Reson. **46**, 435–464 (2015)
48. N. Cox, A. Nalepa, W. Lubitz, A. Savitsky, J. Magn. Reson. **280**, 63–78 (2017)
49. A. Nalepa, M. Malferrari, W. Lubitz, G. Venturoli, K. Mobius, A. Savitsky, Phys. Chem. Chem. Phys. **19**, 28388–28400 (2017)
50. A. Nalepa, K. Möbius, M. Plato, W. Lubitz, A. Savitsky, Appl. Magn. Reson. **50**, 1–16 (2019)
51. K. Möbius, A. Savitsky, M. Malferrari, F. Francia, M.D. Mamedov, A.Y. Semenov, W. Lubitz, G. Venturoli, Appl. Magn. Reson. **51**, 773–850 (2020)

52. A. Savitsky, A. Nalepa, T. Petrenko, M. Plato, K. Möbius, W. Lubitz, Appl. Magn. Reson. **53**, 1239–1263 (2022)
53. M. Plato, H.J. Steinhoff, C. Wegener, J.T. Torring, A. Savitsky, K. Möbius, Mol. Phys. **100**, 3711–3721 (2002)
54. A. Savitsky, A.A. Dubinskii, M. Plato, Y.A. Grishin, H. Zimmermann, K. Möbius, J. Phys. Chem. B **112**, 9079–9090 (2008)
55. P. Gast, R.T.L. Herbonnet, J. Klare, A. Nalepa, C. Rickert, D. Stellinga, L. Urban, K. Möbius, A. Savitsky, H.J. Steinhoff, E.J.J. Groenen, Phys. Chem. Chem. Phys. **16**, 15910–15916 (2014)
56. T. Kawamura, S. Matsunam, T. Yonezawa, Bull. Chem. Soc. Jpn **40**, 1111–1115 (1967)
57. O.H. Griffith, P.J. Dehlinger, S.P. Van, J. Membr. Biol. **15**, 159–192 (1974)
58. B.R. Knauer, J.J. Napier, J. Am. Chem. Soc. **98**, 4395–4400 (1976)
59. A.H. Reddoch, S. Konishi, J. Chem. Phys. **70**, 2121–2130 (1979)
60. L.N. Ikryannikova, L.Y. Ustynyuk, A.N. Tikhonov, J. Phys. Chem. A **108**, 4759–4768 (2004)
61. L.N. Ikryannikova, L.Y. Ustynyuk, A.N. Tikhonov, Magn. Reson. Chem. **48**, 337–349 (2010)
62. S. Sinnecker, E. Reijerse, F. Neese, W. Lubitz, J. Am. Chem. Soc. **126**, 3280–3290 (2004)
63. S. Sinnecker, M. Flores, W. Lubitz, Phys. Chem. Chem. Phys. **8**, 5659–5670 (2006)
64. M. Flores, R.A. Isaacson, R. Calvo, G. Feher, W. Lubitz, Chem. Phys. **294**, 401–413 (2003)
65. M. Flores, R.A. Isaacson, E. Abresch, R. Calvo, W. Lubitz, G. Feher, Biophys. J. **90**, 3356–3362 (2006)
66. M. Flores, R.A. Isaacson, E. Abresch, R. Calvo, W. Lubitz, G. Feher, Biophys. J. **92**, 671–682 (2007)
67. W. Lubitz, G. Feher, Appl. Magn. Reson. **17**, 1–48 (1999)
68. H. Frauenfelder, S.G. Sligar, P.G. Wolynes, Science **254**, 1598–1603 (1991)
69. H. Frauenfelder, G. Chen, J. Berendzen, P.W. Fenimore, H. Jansson, B.H. McMahon, I.R. Stroe, J. Swenson, R.D. Young, Proc. Natl. Acad. Sci. U.S.A. **106**, 5129–5134 (2009)
70. S. Khodadadi, A.P. Sokolov, BBA Proteins Proteom. **1861**, 3546–3552 (2017)
71. K. Henzler-Wildman, D. Kern, Nature **450**, 964–972 (2007)
72. S. Khodadadi, A.P. Sokolov, Soft Matter **11**, 4984–4998 (2015)
73. Y. Levy, J.N. Onuchic, Annu. Rev. Biophys. Biomol. Struct. **35**, 389–415 (2006)
74. H. Frauenfelder, P.W. Fenimore, G. Chen, B.H. McMahon, Proc. Natl. Acad. Sci. U.S.A. **103**, 15469–15472 (2006)
75. Y. Maruyama, Y. Harano, Chem. Phys. Lett. **581**, 85–90 (2013)
76. R.L. Baldwin, Proc. Natl. Acad. Sci. U.S.A. **111**, 13052–13056 (2014)
77. B. Halle, Philos. Trans. R. Soc. Lond. B Biol. Sci. **359**, 1207–1223 (2004)
78. L. Cordone, P. Galajda, E. Vitrano, A. Gassmann, A. Ostermann, F. Parak, Eur. Biophys. J. **27**, 173–176 (1998)
79. G. Palazzo, A. Mallardi, A. Hochkoeppler, L. Cordone, G. Venturoli, Biophys. J. **82**, 558–568 (2002)
80. J.S. Clegg, Comp. Biochem. Physiol. B **128**, 613–624 (2001)
81. F. Francia, M. Dezi, A. Mallardi, G. Palazzo, L. Cordone, G. Venturoli, J. Am. Chem. Soc. **130**, 10240–10246 (2008)
82. L. Cordone, M. Ferrand, E. Vitrano, G. Zaccai, Biophys. J. **76**, 1043–1047 (1999)
83. F. Francia, G. Palazzo, A. Mallardi, L. Cordone, G. Venturoli, Biophys. J. **85**, 2760–2775 (2003)
84. M. Malferrari, A. Savitsky, M.D. Mamedov, G.E. Milanovsky, W. Lubitz, K. Möbius, ASu. Semenov, G. Venturoli, BBA Proteins Proteom. **1857**, 1440–1454 (2016)
85. M.D. Mamedov, G.E. Milanovsky, M. Malferrari, L.A. Vitukhnovskaya, F. Francia, A.Y. Semenov, G. Venturoli, Biochim. Biophys. Acta Bioenerg. **1862**(7), 148413 (2021)
86. J.L. Green, C.A. Angell, J. Phys. Chem. **93**, 2880–2882 (1989)
87. A. Lerbret, P. Bordat, F. Affouard, M. Descamps, F. Migliardo, J. Phys. Chem. B **109**, 11046–11057 (2005)
88. G. Feher, J.P. Allen, M.Y. Okamura, D.C. Rees, Nature **339**, 111–116 (1989)
89. M.M. Leonova, T.Y. Fufina, L.G. Vasilieva, V.A. Shuvalov, Biochem. Moscow. **76**, 1465–1483 (2011)
90. T.L. Olson, J.C. Williams, J.P. Allen, Photosynth. Res. **120**, 87–98 (2014)
91. J.P. Allen, G. Feher, T.O. Yeates, H. Komiya, D.C. Rees, Proc. Natl. Acad. Sci. U.S.A. **84**, 5730–5734 (1987)

92. K.M.R Giangiacomo, D.E. Gunner, L.P. Dutton, Stigmatellin and other electron transfer inhibitors as probes for the Q_B binding site in the reaction center of photosynthetic bacteria, in *Progress in Photosynthesis Research*. ed. by J. Biggins (Springer, Dordrecht, 1987), pp. 409–412
93. G.I. Likhtenshtein, J. Yamauchi, S.I. Nakatsuji, A.I. Smirnov, R. Tamura, *Nitroxides: Applications in Chemistry, Biomedicine and Materials Science* (Wiley-VCH, Weinheim, 2008)
94. W.L. Hubbell, Site-directed spin lableing of membrane proteins, in *Membrane Protein Structure: Experimental Approaches*. ed. by S.H. White (Oxford University Press, London, 1994), pp. 224–248
95. P. Gajula, I.V. Borovykh, C. Beier, T. Shkuropatova, P. Gast, H.J. Steinhoff, Appl. Magn. Reson. **31**, 167–178 (2007)
96. F. Francia, G. Palazzo, A. Mallardi, L. Cordone, G. Venturoli, BB -Proteins Proteom. **1658**, 50–57 (2004)
97. M. Malferrari, F. Francia, G. Venturoli, J. Phys. Chem. B **119**, 13600–13618 (2015)
98. M. Malferrari, A. Nalepa, G. Venturoli, F. Francia, W. Lubitz, K. Möbius, A. Savitsky, Phys. Chem. Chem. Phys. **16**, 9831–9848 (2014)
99. J.A. Rard, J. Solution Chem. **48**, 271–282 (2019)
100. A. Savitsky, M. Malferrari, F. Francia, G. Venturoli, K. Möbius, J. Phys. Chem. B **114**, 12729–12743 (2010)
101. M. Malferrari, F. Francia, G. Venturoli, J. Phys. Chem. B **115**, 14732–14750 (2011)
102. M. Malferrari, A. Mezzetti, F. Francia, G. Venturoli, BBA Proteins Proteom. **1827**, 328–339 (2013)
103. M. Malferrari, G. Venturoli, F. Francia, A. Mezzetti, Spectrosc. Int. J. **27**, 337–342 (2012)
104. M. Plato, E. Tränkle, W. Lubitz, F. Lendzian, K. Möbius, Chem. Phys. **107**, 185–196 (1986)
105. F. Lendzian, W. Lubitz, H. Scheer, C. Bubenzer, K. Möbius, J. Am. Chem. Soc. **103**, 4635–4637 (1981)
106. F. Lendzian, M. Huber, R.A. Issacson, B. Endeward, M. Plato, B. Bönigk, K. Möbius, W. Lubitz, G. Feher, Biochim. Biophys. Acta **1183**, 139–160 (1993)
107. W. Lubitz, F. Lendzian, M. Plato, H. Scheer, K. Möbius, Appl. Magn. Reson. **13**, 531–551 (1997)
108. N. Cox, W. Lubitz, A. Savistky, Mol. Phys. **111**, 2788–2808 (2013)
109. F. Hecker, L. Fries, M. Hiller, M. Chiesa, M. Bennati, Angew. Chem. Int. Ed. Engl. **62**(4), e202213700 (2023)
110. L. Cordone, G. Cottone, S. Giuffrida, G. Palazzo, G. Venturoli, C. Viappiani, BBA Proteins Proteom. **1749**, 252–281 (2005)
111. M.Y. Okamura, M.L. Paddock, M.S. Craige, G. Feher, Biochim. Biophys. Acta Bioenerg. **1458**, 148–163 (2000)
112. A.J. Chirino, E.J. Lous, M. Huber, J.P. Allen, C.C. Schenck, M.L. Paddock, G. Feher, D.C. Rees, Biochemistry **33**, 4584–4593 (1994)
113. J. Koepke, E.M. Krammer, A.R. Klingen, P. Sebban, G.M. Ullmann, G. Fritzsch, J. Mol. Biol. **371**, 396–409 (2007)